Escola Politécnica da Universidade de São Paulo

Gabriel Borba Galvani

Final Graduation Thesis

MICROSCOPIC CHARACTERISATION OF TRIBOSURFACES AFTER PIN-ON-DISC TRIBOTESTING: ALUMINIUM ALLOY VERSUS STEEL, PURE COPPER VERSUS STEEL AND BRASS VERSUS STEEL

São Paulo, 2021

Escola Politécnica da Universidade de São Paulo

Gabriel Borba Galvani

Final Graduation Thesis

MICROSCOPIC CHARACTERISATION OF TRIBOSURFACES AFTER PIN-ON-DISC TRIBOTESTING: ALUMINIUM ALLOY VERSUS STEEL, PURE COPPER VERSUS STEEL AND BRASS VERSUS STEEL

Final Graduation Thesis
Department of Materials and Metallurgical Engineering
Escola Politécnica da Universidade de São Paulo.

Supervisor: Prof. Dr. Cesar Roberto de Farias Azevedo
Co-supervisor: Raphael Oliveira Ferreira

São Paulo, 2021

Catalogação na publicação

Galvani, Gabriel Borba

Microscopic characterisation of tribosurfaces after pin-on-disc tribotesting: aluminium alloy versus steel, pure copper versus steel and brass versus steel -- São Paulo, 2021. 64 p.

Orientador: Cesar Roberto de Farias Azevedo
Coorientador: Raphael Oliveira Ferreira
Trabalho de Formatura – Escola Politécnica da Universidade de São Paulo, Departamento de Engenharia Metalúrgica e de Materiais.

1.Tribologia 2.Cobre 3.Pastilhas de freio 4.Atrito 5.Seleção de materiais 6.Tribofilme 7.Latão 8.Alumínio 9.Triboteste pino versus disco. I.Universidade de São Paulo. Escola Politécnica. Departamento de Engenharia Metalúrgica e de Materiais II.t.

ACKNOWLEDGEMENTS

First of all, I would like to thank Prof. Dr Cesar Azevedo for supporting me in several stages of my formation, from both academic and personal perspectives. I remember how anxious and lost I was when I knocked on his office door to ask for a scientific research project. A few months later, I realised that he was the best professor I ever had at Escola Politécnica da Universidade de São Paulo, besides his “scary beard face”. I am glad that I have had this opportunity to learn a lot with him. He taught me valuable lessons that I will take with me for the rest of my life.

Secondly, I want to thank M.Eng Raphael Oliveira Ferreira for welcoming me to the team project that leads to this present work. If it were not for his patience and didactic, I would struggle to understand many technical concepts of my work. I am glad that our daily routine in the laboratory made us close friends.

I also thank Dra. Ana Cecilia Pontes Rodrigues for helping me with technical questions about my work and always sending me global opportunities to keep developing myself. I am sure that she will help many other students like me in her experience in France.

I would like to thank Escola Politécnica da Universidade de São Paulo for investing in my engineering degree and providing all the technical resources for the present work, especially the Laboratory of Surface Phenomena of the Department of Mechanical Engineering.

Finally, I would like to thank all my friends and professors from the Materials and Metallurgical Department of Escola Politécnica da Universidade de São Paulo, who helped me build who I am today. I know that my academic experience would not be the same if not shared with such great people.

This work would not be possible without the CNPq (*Brazilian National Council for Scientific and Technological Development*) support. I am very grateful for being selected to receive a PIBIC scholarship for the current project.

ABSTRACT

Understanding the properties of copper is critical for the production of efficient brake pads. With the American legislation implying that by 2025 the mass proportion of copper in brake pads should be reduced to a maximum of 0.5% in mass, the need to produce new efficient brake pads has become a priority in the automotive sector.

For this purpose, the current project aimed to characterise the tribological properties of copper, aluminium and brass, when tested against a steel disc on pin-on-disc (PoD) tribotests. Three different normal pressures were applied (0.51 MPa or 10N normal load; 1.02 MPa or 20N normal load and 2.55 MPa or 50N normal load). A tribometer was used to conduct the pin on disc tribotests, providing graphs of the coefficient of friction as a function of the test time for each applied load and material of the pin, performed in triplicate. The tests lasted 3600s, with a rotational speed of 0.1m/s, ambient temperature, and no lubricant.

After the tests, the discs' tribosurfaces were analysed by scanning electron microscopy techniques through secondary electrons (topography image - SE), backscattered electrons (contrast image of chemical composition - BSE), and energy-dispersive X-ray spectrometry (elemental mapping of semi-quantitative chemical composition analysis – EDS). Moreover, the discs' wear tracks were analysed through optical 3D surface interferometry to provide surface parameters related to rugosity. Therefore, it was possible to provide consistent tribological data to develop more efficient and less environmentally harmful brake pads.

Although the brake pad is a polymeric matrix with several constituents, understanding the tribological properties of copper is essential to think of possible substitutes that can provide thermal conductivity and coefficient of friction properties similar to that of copper.

Keywords: Tribology; Copper; Brake pads; Legislation; Materials selection. Tribofilm.

FIGURES LIST

Figure 1: Egyptian illustration, circa 1880a.C. (Bhushan, 2013) 3

Figure 2: Schematic illustration of a tribosystem: I) Interface medium; ll) Contact solids; lll) Mechanical component and its surroundings (J. Halling, 1976). 5

Figure 3: Adhesion observed in friction between two metals (J. Halling, 1976). 5

Figure 4: Increased contact area caused by friction (Stachowiak; Batchelor, 2001). ..6

Figure 5: Representation of the microstructure of a brake pad; note the formation of a third body due to sliding (Österle, 2001). 8

Figure 6: Schematic model of a pin vs disc tribological test (Bhushan, 2013). 10

Figure 7: Bruker tribometer, model DFH 10. 14

Figure 8: Brass pin and steel disc tested under 2.55 MPa (50N normal load). 15

Figure 9: Taylor Robson CCI 3D-profilometer. 17

Figure 10: a) Sa parameter formula and schematic representation. b) Scheme of volume (3D) parameters linked to rugosity analyses. 18

Figure 11: Scanning electron microscope model JEOL JSM 6010LA. 19

Figure 12: Buehler durometer model VMT-3. 20

Figure 13: Coefficient of friction vs time(s) chart for copper pins under 0.51 MPa (10N normal load) (Ferreira, 2017). 24

Figure 14: Coefficient of friction vs time (s) chart for copper pins under 1.02 MPa (20N normal load) (Ferreira, 2017). 25

Figure 15: Coefficient of friction vs time chart for copper pins under 2.55 MPa (50N normal load) (Ferreira, 2017). 25

Figure 16: Average coefficient of friction vs normal load chart for copper pins tests. The respective normal pressures are 0.51 MPa (10N normal load); 1.02 MPa (20N normal load) and 2.55 MPa (50N normal load). (Ferreira, 2017). 26

Figure 17: Coefficient of friction vs time (s) chart for aluminium pins under 0.51 MPa (10N normal load) (Ferreira, 2017). 27
Figure 18: Coefficient of friction vs time (s) chart for aluminium pins under 1.02 MPa (20N normal load) (Ferreira, 2017). 28
Figure 19: Coefficient of friction vs time (s) chart for aluminium pins under 2.55 MPa (50N normal load) (Ferreira, 2017). 28
Figure 20: Average coefficient of friction vs normal load chart for aluminium pins tests The respective normal pressures are 0.51 MPa (10N normal load); 1.02 MPa (20N normal load) and 2.55 MPa (50N normal load) (Ferreira, 2017). 29
Figure 21: Coefficient of friction vs time (s) chart for brass pins under 0.51 MPa (10N normal load) (Ferreira, 2017). 30
Figure 22: Coefficient of friction vs time (s) chart for brass pins under 1.02 MPa (20N normal load) (Ferreira, 2017). 31
Figure 23: Coefficient of friction vs time (s) chart for brass pins under 2.55 MPa (50N normal load) (Ferreira, 2017). 31
Figure 24: Average coefficient of friction vs normal load chart for brass pins tests The respective normal pressures are 0.51 MPa (10N normal load); 1.02 MPa (20N normal load) and 2.55 MPa (50N normal load) (Ferreira, 2017). 32
Figure 25: Tribosurfaces of steel discs before tests (500x amplification). a) SE detector image for topographic contrast. b) BSE detector image for atomic weight contrast (Ferreira, 2017). 34
Figure 26: Tribosurfaces of steel discs after tests with copper pins under 2.55 MPa or 50N normal load (500x amplification). a) SE detector image for topographic contrast. b) BSE detector image for atomic weight contrast. c) Composition map for iron. d) Composition map for copper. e) Composition map for oxygen (Ferreira, 2017). 36

Figure 27: Chart of oxygen and copper atomic composition of the disc tribosurface as a function of normal loads for steel-copper tribopair tests. The respective normal pressures are 0.51 MPa (10N normal load); 1.02 MPa (20N normal load) and 2.55 MPa (50N normal load). Data from EDS analysis under 20 kV tension, 30 min duration and 20% dead time (Ferreira, 2017). 37
Figure 28: Tribosurfaces of steel discs after tests with aluminium pins under 2.55 MPa or 50N normal load (500x amplification). a) SE detector image for topography contrast. b) BSE detector image for atomic weight contrast. c) Composition map for iron. d) Composition map for aluminium. e) Composition map for oxygen (Ferreira, 2017)..... 39
Figure 29: Chart of oxygen and aluminium atomic composition of the disc tribosurface as a function of normal loads for steel-aluminium tribopair tests. The respective normal pressures are 0.51 MPa (10N normal load); 1.02 MPa (20N normal load) and 2.55 MPa (50N normal load). Data from EDS analysis under 20 kV tension, 30 min duration and 20% dead time (Ferreira, 2017). 40
Figure 30: Tribosurfaces of steel discs after tests with brass pins under 2.55 MPa or 50N normal load (500x amplification). a) SE detector image for topographic contrast. b) BSE detector image for atomic weight contrast. c) Composition map for iron. d) Composition map for copper. e) Composition map for zinc. f) Composition map for oxygen (Ferreira, 2017). 42
Figure 31: Chart of oxygen, copper and zinc atomic composition of the disc tribosurface as a function of normal loads for steel-brass tribopair tests. The respective normal pressures are 0.51 MPa (10N normal load); 1.02 MPa (20N normal load) and 2.55 MPa (50N normal load). Data from EDS analysis under 20 kV tension, 30 min duration and 20% dead time (Ferreira, 2017). 43

Figure 32: 2D profiles obtained in an analysis in the rugosimeter. The top image represents a point in which the wear line is parallel to the grinding lines, while the bottom figure represents a point in which lines are perpendicular. 44
Figure 33: Rugosimeter results for copper pins under 2.55 MPa (50N normal load). 45
Figure 34: Rugosimeter results for aluminium pins under 2.55 MPa (50N normal load).....46
Figure 35: Rugosimeter results for brass pins under 2.55 MPa (50N normal load)...47
Figure 36: Chart of mean Sa as a function of normal loads for each tribopair (aluminium in blue, copper in orange and brass in grey). The respective normal pressures are 0.51 MPa (10N normal load); 1.02 MPa (20N normal load) and 2.55 MPa (50N normal load). 49
Figure 37: Chart of mean Vmp in function of normal loads for each tribopair (aluminium in blue, copper in orange and brass in grey). The respective normal pressures are 0.51 MPa (10N normal load); 1.02 MPa (20N normal load) and 2.55 MPa (50N normal load). 49
Figure 38: Chart of mean Vvv as a function of normal loads for each tribopair (aluminium in blue, copper in orange and brass in grey). The respective normal pressures are 0.51 MPa (10N normal load); 1.02 MPa (20N normal load) and 2.55 MPa (50N normal load) 50
Figure 39: Evolution of the coefficient of friction in the tribological pin versus disc test in aluminium-steel tribological pair with a normal load of 10N and relative humidity of 70%. (Chowdhury et al., 2011) 51
Figure 40: Plots of total material wear volume versus oxygen diffusion coefficient at 293K temperature for different oxides. (Kato, 2007) 54

Figure 41: Plots of total material wear volume versus sliding distance for different oxides under 35N normal load.. (Kato, 2007) 55

TABLES LIST

Table 1: PMC brake pad composition (Kukustchova, 2009). 8

Table 2: EDS microanalyses of the 4140 steel disc. 22

Table 3: EDS microanalyses of the C10200 copper pin 22

Table 4: EDS microanalyses of the C36000 brass pin 22

Table 5: EDS microanalyses of the 6082-T6 aluminium pin 23

Table 6: Specified (upper line) and measured (lower line) Vickers hardness values. 23

Table 7: Specified thermal conductivities of the tested samples (Edupack, 2015). ... 23

Table 8: Mean coefficients of friction for each pin material and normal pressure. 33

Table 9: 2D and 3D rugosity parameters obtained for 2.55 MPa (50N normal load), in perpendicular and parallel directions, for aluminium, copper and brass pins. Two different points were analysed. 48

Table 10: Mean of rugosity parameters obtained for 2.55 MPa (50N normal load), in perpendicular and parallel directions, for aluminium, copper, and brass pins. Also, a column with the total mean was added. 48

Table 11: Mean mass losses for each pin material and normal load. 53

Table 12: Non-exhaustive list of proposed copper-free formulations in both market and industrial levels. 58

Summary

1. INTRODUCTION....3
1.1. Tribology....3
1.2. Copper in automotive brake systems....7
1.3. Pin-on-disc tribotest....10
1.4 Justification....11
1.5. Objectives....12
2. METHODOLOGY....13
2.1. Samples....13
2.2. Tribological tests....13
2.3. Tribosurfaces characterisation....16
2.3.1. Optical 3D surface interferometry characterisation....16
2.3.2. SEM characterisation....19
2.4. Data treatment....20
2.4.1. Hardness of samples....20
2.4.2. Coefficient of friction plots....21
3. RESULTS....22
3.1. Samples' specifications....22
3.2. Coefficient of friction (CoF) plots....24
3.2.1. Copper pins....24
3.2.2. Aluminium pins....27
3.2.3. Brass pins....30
3.3. Consolidated results of the mean coefficients of friction....33
3.4. Microscopic characterisation of steel discs´ tribosurface after tribotesting....34
3.4.1. Initial condition of the steel discs' tribosurfaces....34
3.4.2. Microscopy and chemical composition for 2.55 MPa tests (copper-steel pair)....35

3.4.3. Microscopy and chemical composition for 2.55 MPa tests (aluminium-steel pair) 38
3.4.4. Microscopy and chemical composition for 2.55 MPa tests (brass-steel pair) 41
3.5. Analyses of the disc surfaces in the rugosimeter 44
3.5.1. Effect of disc grinding on surface analysis 44
3.5.2. Results for tribotests with copper pins (2.55 MPa) 45
3.5.3. Results for tribotests with aluminium pins (2.55 MPa) 46
3.5.4. Results for tribotests with brass pins (2.55 MPa) 47
3.5.5. Consolidated results of surface parameters 47
4. DISCUSSION 51
4.1.1. Coefficient of friction 51
4.1.2. Mass variation of pins 53
4.1.3. Tribological mechanisms 54
4.1.4. Final remarks, the future of copper-free brake pads 57
5. CONCLUSIONS 59
6. REFERENCES 60

1. INTRODUCTION

1.1. Tribology

Tribology can be defined as the study of friction, wear, and lubrication between two surfaces that interact in relative motion. It was defined as a new branch of science in 1967 by the Organization for Economic Cooperation and Development (OECD) committee. The name is derived from Greek, in which the word “tribes” means slip (Stachowiak, Batchelor, 2001). Although this vast area of material science started to be recorded only in the second half of the 20th century, there are many documented examples of how ancient civilisations developed rolling surfaces with low coefficient of friction (CoF). For example, older documents indicate that in 3500 BC. the use of wheels was already a reality, which shows the concern of our ancestors with the reduction of friction and consequently of energy losses in translational movement. An 1880 BC illustration in Egypt (Figure 1) reveals men dragging a 600kN statue along a wooden path. Upon the statue’s support, a man pours a liquid into the track of the movement, probably intending to ease the friction between the sleigh and the ground to reduce the force needed to be applied by each man. That may have been one of the first lubrication engineers in history (Bhushan, 2013).

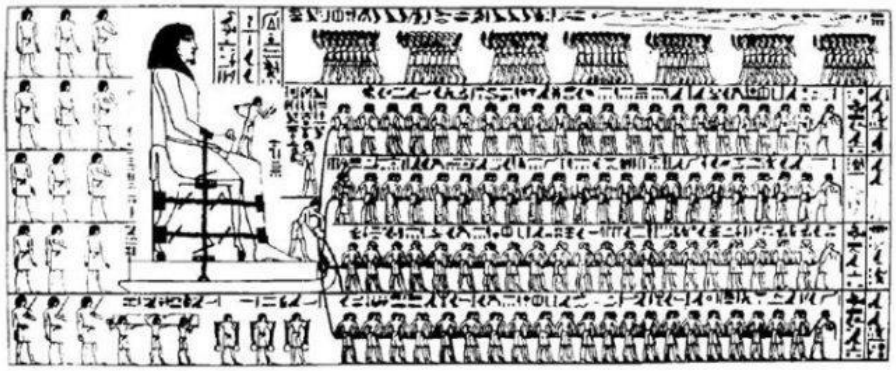

Figure 1: Egyptian illustration, circa 1880a.C. (Bhushan, 2013)

According to estimates, the losses stemming from ignorance about tribology in the United States amount to 4% of its gross domestic product (approximately $200 billion per year in 1966), and approximately one-third of the world’s energy resources appear in the form of friction in one way or another. Thus, the importance of reducing friction and controlling wear is related to economic reasons and long-term reliability. According to Jost (1966, 1967), it is possible to save around 1% of a nation’s gross domestic product by implementing better tribological practices. The economy is both

substantial and significant and could be obtained without the employment of a large invested capital (Bhushan, 2013).

With the emergence of new experimental techniques such as microscopy, the perceptions of changing the structures of solid surfaces and interfacial media between them made us rethink the basic concepts of friction. The advancement of fine-scale techniques has led researchers to consider friction as a relevant variable in their studies. (Blau, 1996). It is then evident the importance of tribology to society, as its study allows for better performance, failures reduction, and considerable savings. Moreover, in comparison, many basic engineering materials such as thermodynamics, mechanics, and plasticity are relatively old and well established, while the tribology domain still presents controversies and is a branch to be better explored. (Stachowiak, 2001). In the late 20th century, the coefficients of static and kinetic friction have been recognised to be both material and system dependent, and the term “tribological system” was first used to define the complex variety of phenomena and parameters that control the coefficient of frictions and wear properties (Czichos, 1980).

Figure 2 shows a hierarchy scheme of the factors acting at each level of interaction in the tribosystem (Blau, 1996). The Interfacial medium (I) involves lubrication theories, tribochemical films and triboparticles. Contact solids (II) involves theories of deformation, fracture, fatigue, material interaction/medium, and material transfer; (III) Mechanical component and its surroundings: related to the dynamics of the component (Blau, 1996). The study of tribological systems became a modern tool for interpreting and modelling friction, developing materials that control the coefficient of friction (CoF); to develop tests and methods to characterise friction, and developing machinery (Blau, 1996).

In the study of wear, it is essential to recognise that several independent mechanisms are involved. Burwell listed four wear types in the “Search for Possible Wear Mechanisms”: slip wear (or adhesive), abrasive wear, corrosive wear, and surface fatigue. It also included a fifth classification named “minor wear types”, including erosion, cavitation, and impact roughing (J.Halling,1976). Macroscopically, surfaces that are considered smooth are rough on the atomic scale, and the contact between two surfaces happens on only a few roughnesses. With a normal load application, the local pressure in the asperities becomes extremely high. The flow limit is exceeded, and the asperities deform plastically until the contact area increases

sufficiently to support the applied load. In the absence of surface films, surfaces would be adhered to, but small amounts of contaminants prevent adhesion from occurring purely under normal load (J. Halling, 1976). Numerous tests using a variety of metal combinations have shown that when there is high adhesion, the material transfer occurs from the weaker material to the stronger material, as illustrated in Figure 3. However, a relative tangential movement at the interface can occur to disperse the contaminant films at the contact points, and cold welding of the junctions occurs. Continuous slip can lead to homogeneity, and more junctions may be formed (J. Halling, 1976).

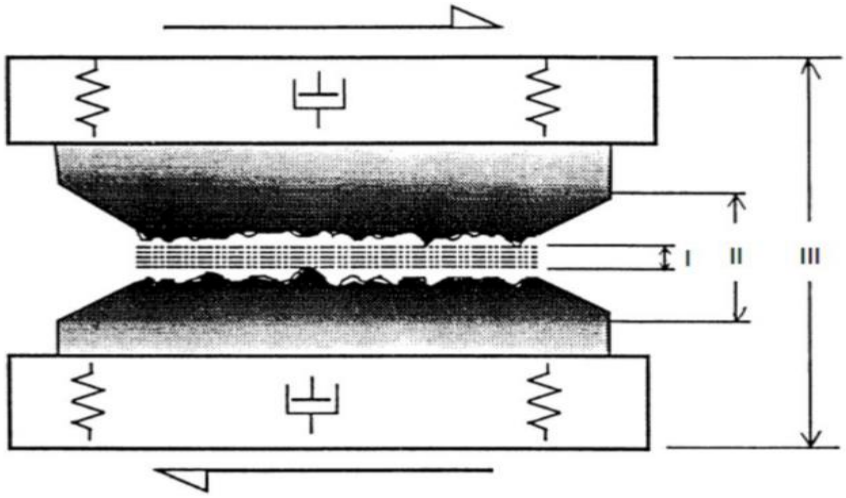

Figure 2: Schematic illustration of a tribosystem: I) Interface medium; II) Contact solids; III) Mechanical component and its surroundings (J. Halling, 1976).

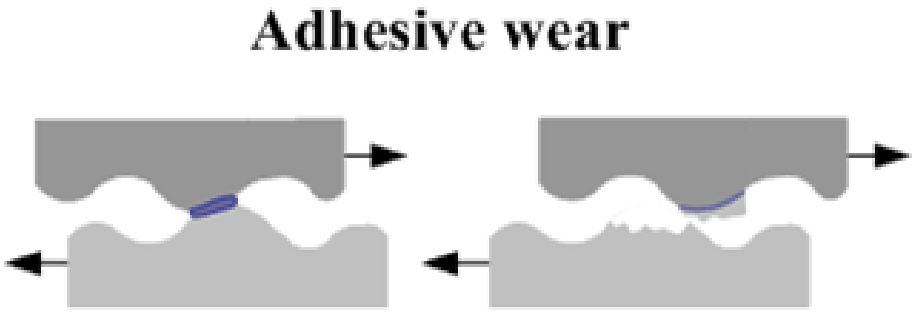

Figure 3: Adhesion observed in friction between two metals (J. Halling, 1976).

The increased contact area reduces the normal pressure (the same load now acts on a larger area), as illustrated in Figure 4. The tangential force and contact area grow until the value of the shear module is maximum. This implies that each contact point is under maximum stress during sliding conditions before the shear break. As a result, the coefficient of friction also increases as the system instability increases.

(Stachowiak, Batchelor, 2001). The high adhesion observed between metals can be explained by the transfer of electrons between contact surfaces. Metals have free electrons and, on contact, electrons exchange to establish the bond. As a result, electrons can bind two solids despite their different atomic structures (Stachowiak, Batchelor, 2001).

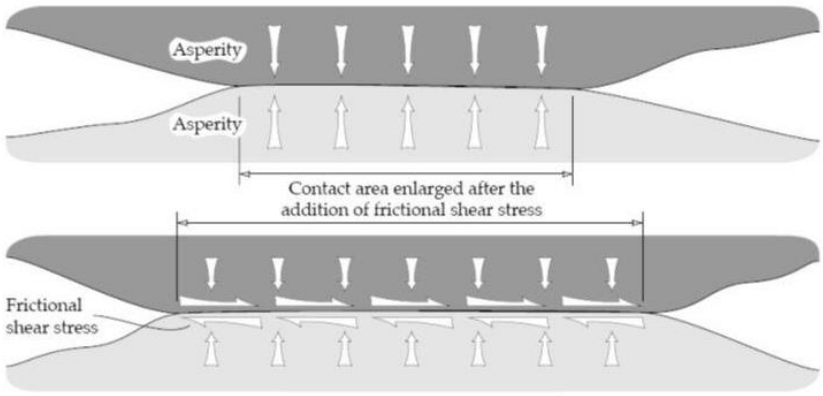

Figure 4: Increased contact area caused by friction (Stachowiak; Batchelor, 2001).

1.2. Copper in automotive brake systems

A brake system provides a way to convert kinetic energy into heat. The heat generated at the sliding interface of the brake system is dissipated primarily by driving through the brake components. There are two main brake systems available for automobiles: disc and drum systems (Jacko, 1984 and Blau, 1996). During braking, the coefficient of friction needs to be suitable and stable in high operating speeds, applied pressures, and temperatures. A particular interest is the ability of the insert disc and materials to resist the deterioration caused by friction when they need to hold to extreme temperatures during service, which can reach a temperature of up to 800oC (thermal stability). An important project requirement is the ability to withstand high temperatures caused by friction, so the disc must have enough thermal storage capacity and good thermal conductivity to prevent distortion, thermal fatigue or cracking due to thermal stresses (Maleque, 2010). Brake materials have other requirements such as good compressive and shear resistance, corrosion resistance, light, wear-resistant, and cost. The most common material for discs of brake systems is perlite grey cast iron, while the brake pads are a complex polymeric matrix composite (PMC). Disc brake systems produce a braking force by pressing the brake pads on the disc. The higher the dynamic coefficient of friction between these components, the more energy is generated in the brake, although this value may vary with the design and operating parameters (Jacko, 1984 and Blau, 1996).

When the surface of a PMC type brake pad slides against the disc, there is a reduction in the surface roughness of the disc until it reaches a stable value. During this transition period, the coefficient of friction varies significantly. Similarly, the wear level is continuously reduced until it achieves an equilibrium value. Once this equilibrium is reached, there are continuous and uniform tribofilms in the tribosurfaces of the disc and pad. Different constituents are present in a brake pad, and its composition and microstructure mainly control the braking performance. The most common constituents are ceramic particles and fibres, minerals, metallic chips, solid lubricants and elastomers dispersed in a phenolic resin matrix, as shown in Figure 5 (Osterle, 2001). Table 1 shows the composition of a given PMC brake pad. For this particular PMC described by Kukustchova (Kukustchova, 2009), copper represented 4% weight of the total composition. However, this value can vary between different fabricants.

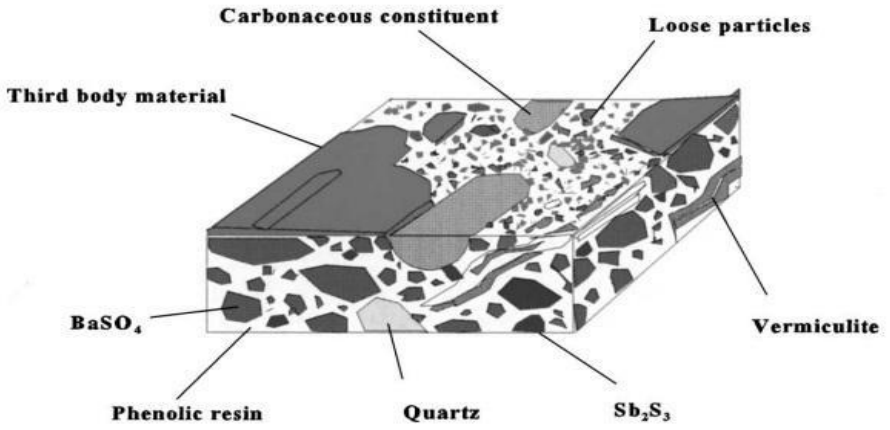

Figure 5: Representation of the microstructure of a brake pad; note the formation of a third body due to sliding (Österle, 2001).

Table 1: PMC brake pad composition (Kukustchova, 2009).

Constituent	Volume %	Weight %
Steel Fiber	2.7	10
Synthetic Graphite	4.8	5
Resilient Graphitic Carbon (RGC)	5.3	5
Coke	16.8	15
Iron Powder	2.6	3
Vermiculite	3.5	5
$ZrSiO_4$	0.9	2
Nitrile Rubber (NBR)	8.5	5
Twaron	3.0	2
$BaSO_4$	6.6	9
Copper	0.9	4
MgO	3.3	3
Sb_2S_3	1.0	3
Tin	1.6	3
MoS_2	0.4	1
Al_2O_3	1.4	1
Phenolic Resin	36.5	24

Among many other ingredients, copper particles/fibres are currently used in the automotive brake pads. Although with some variations, most brake pads have copper or brass particles or a combination of both. However, there is growing concern about the use of copper due to its environmental impacts, leading to an increasing demand on the automotive industry to decrease its use (Österle, Prietzel, Kloß & Dmitriev, 2010). The main reason for the use of copper is its excellent thermal conductivity, avoiding localised overheating of the tablets. In addition, these copper particles that make up the brake pads serve as mechanical reinforcements due to the hardening that these particles suffer from interlocking in the braking operations, which induce the formation of nanocrystalline structure in the particles. In addition, when the

temperature increases, copper also acts as a material that softens braking and reduces noise. With the increase in temperature and wear of copper particles in contact with the disc, copper nanoparticles are incorporated into the iron-oxide rich tribofilm (Österle et al., 2010).

There are already several copper-free claimed formulations for brake pads in the automotive market. Bosch developed the QuietCast, a copper-free ceramic brake pad produced from special aerospace alloy with a higher content in aluminium. This new formulation could reduce up to 8% of an average copper-full brake pad weight and extend its life by 17% (Bosch, 2021). Fras-le released the GRN Tech, manufactured from a highly durable formulation, currently being tested in the US, Europe, and Brazil with positive results. Claimed to be a global leader in brake technology and innovation, the company is among the top five manufacturers of friction materials in the world (Fras-le, 2021). Finally, Hella Pagid released its copper-free formulation, complying with the OE quality standards. The company aims at offering solely copper-free brake pads already before the law's coming-into-effect in the year 2025 (Hella Pagid, 2021). Although these companies promise "environmentally friendly" Cu-free brake pads and efficiency gains compared to Cu-full brake pads, it is not clear how true this is. On their websites (Bosch, 2021; Fras-le, 2021; Hella Pagid, 2021), no information is disclosed regarding their environmental impacts and efficiency in performance. Recent studies showed that Cu-free brake pads emit more airborne particles than Cu-contained brake pads (Olofsson et al., 2020). Said so, new formulations must be developed and characterised to avoid that possible harmful formulation being released into the market.

1.3. Pin-on-disc tribotest

Numerous specific tests to measure friction, based on simulating applications and problems, have been developed. Traditional laboratory-scale tests produce a contact between surfaces with a few square millimetres, but large dynamometers measure friction forces in train brake pads with tens of square centimetres of area. Each technique and method has its place in triboscience and tribotechnology (Blau, 1996). The tribological behaviour of different materials and lubricants often needs to be studied to develop new components. Other tests may be conducted for quality control to determine the service life, reliability, or intervals required for in-service maintenance. The influence of service variables can be favourably investigated in model tests, subcomponent tests, or component tests. The results of the tribological tests can improve the design of new components. The simulation of complex systems by a relatively simple model is essential for studying the basic mechanisms of friction, lubrication, and wear. (Zum Gahr, 1987). In the pin-on-disc tribotesting, the pin is kept still, and the disc rotates, as shown in Figure 6. The pin can be a non-rotating sphere, a rectangular parallelepiped, or a flat-faced cylinder. This test is probably the most commonly used during the development of new friction materials for tribological applications (Bhushan, 2013).

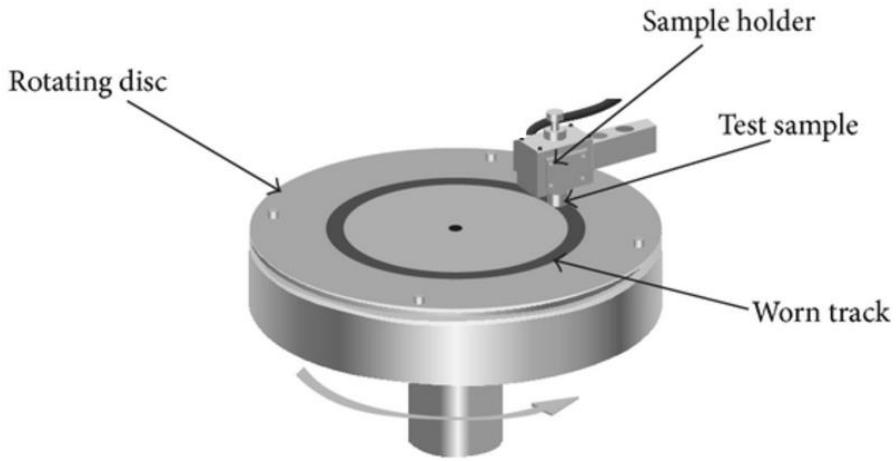

Figure 6: Schematic model of a pin vs disc tribological test (Bhushan, 2013).

1.4 Justification

In the United States, concerns about emissions of fine and ultra-fine copper particles into the air have led to a change in legislation to reduce the use of copper in brake pads by 2025 to 0.5% in mass weight (California Department of Toxic Substances Control, 2016). Scientific research has confirmed the relationship between exposure to copper particles in the air and respiratory diseases, leading to cardiopulmonary death. It has been reported that more than 50% of the particles produced by braking are carried by air in the form of 20 nm fine nanoparticles. Copper fibres are usually present in brake pads in mass fractions between 10% and 15% (Kukutschova, 2009). In addition, aquatic life is also affected by the emission of copper particles. In rainy times, copper particles present in the air are carried to rivers, seas, and lakes. In 2010, the US Environmental Protection Agency estimated that 590 tons of copper were released into the environment in California. Copper is toxic to many aquatic species and the fact that it harms fish's olfactory system, thus reducing their chances of survival. (California Department of Toxic Substances Control, 2016). Since the mid-1970s, researchers have been looking for new compositions for brake pads and the industry is finding new compositions and microstructures, which promote the formation of stable tribofilms under working conditions. There is a desire to find lighter materials with higher performance at high temperatures, better performance, and that produce fewer particles that are harmful to the environment. (Jacko, 1984 and Abbasi, 2011). To replace Cu in the brake pad, researchers need to fully understand its behaviour during dry sliding. This area of study can attract the attention of many automobile companies to find a replacement for the height of copper in the brake pads.

1.5. Objectives

Considering the current need to produce copper-free brake pads, the general objectives of this work are:

- Evaluate the CoF evolution during pin on disc tribotest under 3 different normal loads and using 3 metals as pin materials with similar hardness and high thermal conductivity (copper, aluminium and brass) tested against steel discs;
- Provide a topographic characterisation of the discs' tribosurfaces formed after the tests by 3D profilometry technique to collect different surface parameters (arithmetical mean height; dale void volume and peak material volume);
- Provide a microscopic characterisation of the disc's tribosurfaces by using three scanning electron microscopy techniques: secondary electrons (topography 2D image - SE), backscattered electrons (contrast image of chemical composition - BSE), and energy-dispersive X-ray spectrometry (elemental mapping of semi-quantitative chemical composition analysis – EDS).
- Evaluation of the mass variation of the pins after the tests to quantify wear;
- Compare and discuss all tribopairs regarding their tribological behaviours.

That way, a better understanding of the role of copper in brake pads can be provided through a comparative analysis with other metals.

2. METHODOLOGY

The tribotests and microscopic examinations were conducted at the Laboratory of Surface Phenomena of the Department of Mechanical Engineering of Escola Politécnica da Universidade de São Paulo. This research project was financially supported by CNPq Institutional Scientific Initiation Scholarship Program (PIBIC)*:* project number 800585/2016-0, active from 01/08/2017 to 31/07/2018, named *"Ensaios Tribológicos do tipo pino versus disco para quatro pares metálicos: caracterização microestrutural dos tribolfimes e tribosuperfícies"* (Galvani, 2017) It was carried out in conjunction with the master's thesis of Raphael Oliveira Ferreira (Ferreira, 2017). Thus, some of the results were shared and already published in both projects.

2.1. Samples

The tested samples were 5 mm thick and 80 mm diameter ground AISI 4140 steel discs and 5 mm diameter and 20 mm height pins made of C10200 copper, 6082-T6 aluminium and C36000 brass. The selection of the pin materials was performed with the CES Edupack 2015 software in the level 3 database (Edupack, 2015) and imposing three restrictions: non-ferrous metals with thermal conductivity above 100 W/m.°C and with values of hardness between 90 and 110 HV.

2.2. Tribological tests

Before the tests, the pins were sanded using circular silicon carbide sandpapers with granulometries of #180, #400 and #600. The pins and discs were cleaned immersed in alcohol in the ultrasound for 20 minutes, and their masses were measured in an analytical balance Mettler Toledo model XP205 (millimetric precision) before and after tests (5 measurements were made, the mean and standard deviation were calculated). The tests have been carried out in a Bruker tribometer Bruker, model DFH 10 (see Figure 7) under the ASTM G99 (ASTM, 2011) norms and the following conditions:

- Duration: 60 min
- Rotational speed: constant at 0.1 m/s
- Tests in triplicate
- Ambient temperature (10°C – 25°C)

- Humidity: not measured
- Absence of lubricant
- Nominal contact pressures around 0.51 MPa (10N normal load); 1.02 MPa (20N normal load) and 2.55 MPa (50N normal load).

Figure 7: Bruker tribometer, model DFH 10.

In summary, 27 steel discs and 9 pins of each composition (copper, aluminium, and brass) were used. Figure 8 shows an example of a steel disc and a brass pin after a tribotest, with a visible wear track.

Figure 8: Brass pin and steel disc tested under 2.55 MPa (50N normal load).

2.3. Tribosurfaces characterisation

After the tribological tests, the discs were cleaned immersed in alcohol in the ultrasound for 20 minutes. Furthermore, the discs' tribosurfaces were analysed by a scanning electron microscope and an optical 3D surface interferometer. The analyses conditions are detailed below.

2.3.1. Optical 3D surface interferometry characterisation

A 3D non-contact surface profiler uses a range of optical acquisition methodologies to obtain surface topography information from a surface. These methods typically scan a surface with an incident light source and measure the emissive, reflective, or refractive light to acquire information about the product's surface topography. This metrological method is often preferred over contact surface profiling due to its low invasiveness and improved measurement speeds (Taylor Hobson, 2018).

For this project, a profilometer 3D CCI Taylor Hobson was used (see Figure 9). The Taylor Hobson Calibration Laboratory calibrated it on 04/19/2017, calibration certificate number 54407. A light level of 50% was set, with 10x magnification, a working distance of 7.4 mm, XY analysis mode, analysis speed of 5x. The analysis was made in the cross-section of the disc's wear track with an area of 1.4 by 7.0 mm for each measurement.

Figure 9: Taylor Robson CCI 3D-profilometer.

This technique was used to produce three-dimensional images of the topography of the wear track of the disc on a microscopic scale. It has been very relevant to the project, considering that the SEM can only produce two-dimensional images. A table of ISO 25178-2 standard (ISO, 2012) describes the main surface parameters that were used in the analysis and they are represented in Figure 10.

- **Sa**: Arithmetic Mean of the height in a module of a surface, measured in µm. Sa is commonly related to roughness.
- **Vmp:** Peak Material Volume, is the volume of material comprising the surface from the height corresponding to a material ratio level, “p”, to the highest peak, measured in $\mu m^3/\mu m^2$. The default value for “p” is 10%.
- **Vvv:** Dale Void Volume, is the volume of space bounded by the surface texture from a plane at a height corresponding to a material ratio (mr) level, “p” to the lowest valley, measured in $\mu m^3/\mu m^2$. The default value for “p” is 80%. The Vmp/Vvv ratio is related to adhered/worn volume.

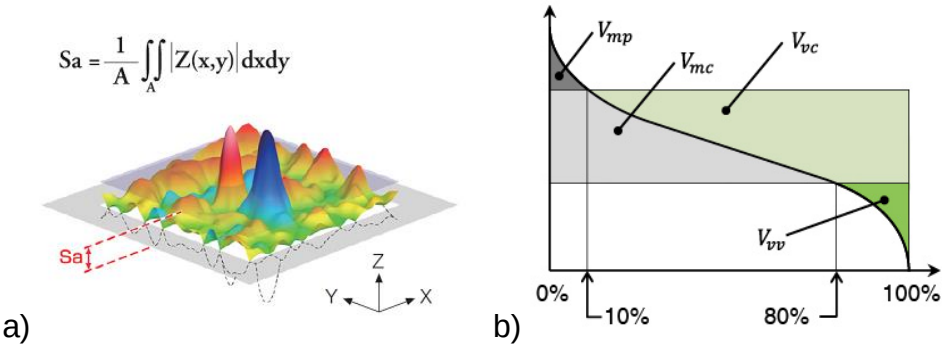

Figure 10: a) Sa parameter formula and schematic representation. b) Scheme of volume (3D) parameters linked to rugosity analyses.

These analyses provided three-dimensional images of the tribosurfaces, allowing the superficial characterisation using different parameters (3D optical interferometry). The variations in volume and topographic profile on the wear track could be obtained.

2.3.2. SEM characterisation

A Scanning Electron Microscope (SEM) is an electron microscope that uses a focused beam of electrons that react with the sample to produce a topological image and relative composition. Upon contact with the sample, the focused beam of electrons produces secondary electrons (SEs), backscattered electrons (BSEs), and characteristic X-ray, which is then detected with respective detectors and finally displayed on the monitor. EDS spectroscopy is involved in the detection of these characteristic X-rays to provide an elemental composition of the analysed surface (Mutalib, M.A. et al.,2017)

The tribosurfaces of the discs were analysed after testing in the scanning electron microscope JEOL JSM 6010LA (see Figure 11) through secondary electrons (topography image - SE), backscattered electrons (contrast image of chemical composition - BSE), and energy-dispersive X-ray spectrometry (semi-quantitative chemical composition analysis – EDS). Images were acquired with amplification of 500 times. The chemical composition microanalyses were made with an acceleration voltage of 20kV and dead time of 20%. The average time of chemical analysis for the mapping of chemical composition was 30 minutes. With the assistance of a laboratory expert, the acceleration voltage of the electron beam, as well as the beam diameter (“spot size”), the focus (“working distance”), and other operating parameters have been regulated for each sample type.

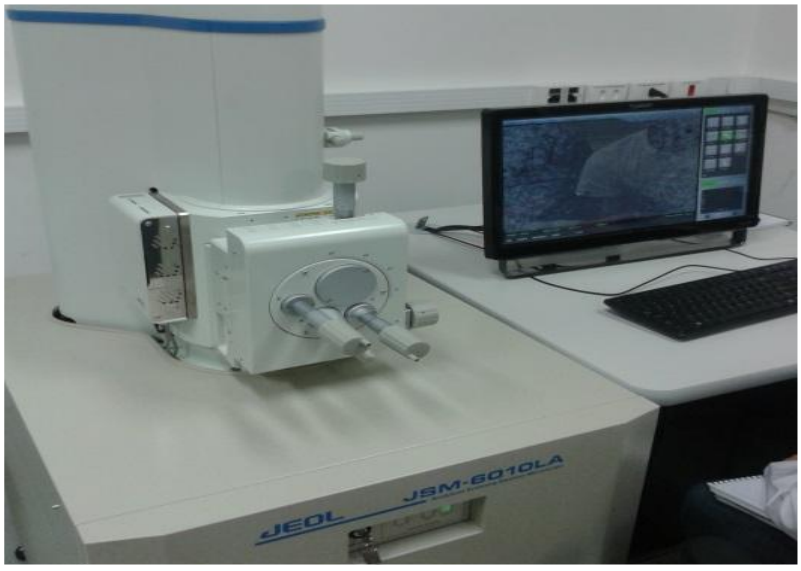

Figure 11: Scanning electron microscope model JEOL JSM 6010LA.

2.4. Data treatment

2.4.1. Hardness of samples

A Buehler model VMT-3 was used in this project (see Figure 12) to measure the hardness of the discs and pins. It was calibrated by the company Holtermann Commercial and Technical on 08/11/2017, calibration certificate number 22107/17. The Vickers Hardness (HV) is calculated by optically measuring the diagonal lengths of the impression left by the indenter of the durometer, which converts these measures into hardness measures in the calibrated equipment (Struers, 2021). Before the tests, the measured Vickers hardness values of the pin and disc materials were compared with those specified by the EN standards and presented in CES Edupack 2015 Level 3 software (Edupack, 2015) to verify that they were within the specifications and suitable for what was specified for the tests. A load of 30 kgf was used to measure the hardness of the discs, and five measurements were made on the surface of each disc to calculate the mean value and standard deviation. The pins were sanded using silicon carbide in the following granulometry sequence: #220, #400 and #600 before the hardness measurements were made. Five measurements were performed for each material, with a load application of 10 kgf to calculate the mean value and standard deviation.

Figure 12: Buehler durometer model VMT-3.

2.4.2. Coefficient of friction plots

The Bruker tribometer shown previously in Figure 7 was configured for data acquisition at a frequency of 100Hz. The results were extracted in text files with an average filter of every hundred points. The CoF graphics were plotted using Origin 8.5 software at 1 point per second. The coefficient of friction was plotted as a function of time for each material triplicate. A mean coefficient of friction and its standard deviation of each triplicate was calculated (range between 500 and 3600 seconds) for each normal load applied and pin material.

3. RESULTS

3.1. Samples' specifications

Tables 2 to 5 show the chemical compositions of the materials specified by the EN standards, obtained in the CES Edupack 2015 software level 3 database (Edupack, 2015), and the EDS microanalyses. The 4140 steel disc had manganese content above the specified in the EN 42CrMo4 specification. The C10200 copper pin presented the copper content compatible with that specified by the EN standard CW008A. The C36000 brass pin did not detect iron content, and the lead content found was below that specified by EN CW603N. The chemical composition measured through the semi-quantitative microanalysis suggests a chemical composition closer to the brass alloy C36500, known as Muntz Metal, which has lead content between 0.25 and 0.7% by weight and copper content close to that measured in the semi-quantitative measurement. The 6082-T6 aluminium pin had a silicon content above that specified by EN AW-6082 and no iron was detected.

Table 2: EDS microanalyses of the 4140 steel disc.

Steel AISI 4140	**Fe (% atm)**	**Si (% atm.)**	**Mn (% atm.)**	**S (% atm.)**	**Cr (% atm.)**	**Mo (% atm.)**
Specification (EN Edupack)	96.8 – 97.8	0.15 – 0.35	0.75 - 1	0 – 0.04	0.8 – 1.1	0.15 – 0.25
Measured (EDS)	97.2	0.2	1.4	0.1	1.1	0.1

Table 3: EDS microanalyses of the C10200 copper pin

Copper C10200	**Cu (% atm.)**
Specification (EN Edupack)	100
Measured (EDS)	100

Table 4: EDS microanalyses of the C36000 brass pin

Brass C36000	**Cu (% atm.)**	**Zn (% atm.)**	**Pb (% atm.)**	**Fe (% atm.)**
Specified (EN Edupack)	60.0 – 63.0	The rest	2.5 – 3.0	0 – 0.35
Measured (EDS)	62.9	36.1	0.8	-

Table 5: EDS microanalyses of the 6082-T6 aluminium pin

Aluminium 6082-T6	Al (% atm.)	Si (% atm.)	Mg (% atm.)	Mn (% atm.)	Fe (% atm.)
Specified (EN Edupack)	97	0,7 – 1.3	0.6 – 1.2	0.4 – 1.0	0 – 0.5
Measured (EDS)	95.6	1.7	0.9	0.7	-

Vickers hardness measures conducted in the durometer are shown in Table 6. The C10200 copper and 6082-T6 aluminium pins presented hardness values within the EN CW008A and EN AW-6082-T6 specifications. The 4140 steel disc had hardness approximately 24 HV below the EN 42CrMo4 specification, and the C36000 brass pin had hardness approximately 9 HV below that specified by EN CW603N.

Table 6: Specified (upper line) and measured (lower line) Vickers hardness values.

Steel 4140	Copper C10200	Brass C36000	Aluminium 6082-T6
183 – 223 HV	80 – 115 HV	105 – 140 HV	95 – 105 HV
159 ± 2 HV30	101 ± 2 HV10	96 ± 3 HV10	104 ± 3 HV10

Table 7 summarises the specified thermal conductivities of the disc and each pin material (Edupack, 2015). An important project requirement for brake pads is the ability to withstand high temperatures caused by friction, so braking materials must have enough good thermal conductivity to prevent distortion, thermal fatigue or cracking due to thermal stresses (Maleque, 2010). No measures were conducted in that case.

Table 7: Specified thermal conductivities of the tested samples (Edupack, 2015).

Steel 4140	Copper C10200	Brass C36000	Aluminium 6082-T6
42 – 48 W/m.°C	390 – 398 W/m.°C	115 – 121 W/m.°C	169 – 175 W/m.°C

3.2. Coefficient of friction (CoF) plots

3.2.1. Copper pins

Figures 13, 14 and 15 show the coefficient of friction versus test time for each repetition, using copper pins under different normal loads. The behaviour of the coefficient of friction was considered unstable. For the three loads, the mean values ranged between 0.6 and 0.7. The increase in normal load decreased the mean point oscillation of the coefficient of friction (the range of values reached). For 0.51 MPa (10N normal load), the mean point oscillation was 0.3. For 1.02 MPa (20N normal load), it was 0.2. The CoF oscillation was much lower for 2.55 MPa (50N normal load), varying only 0.05.

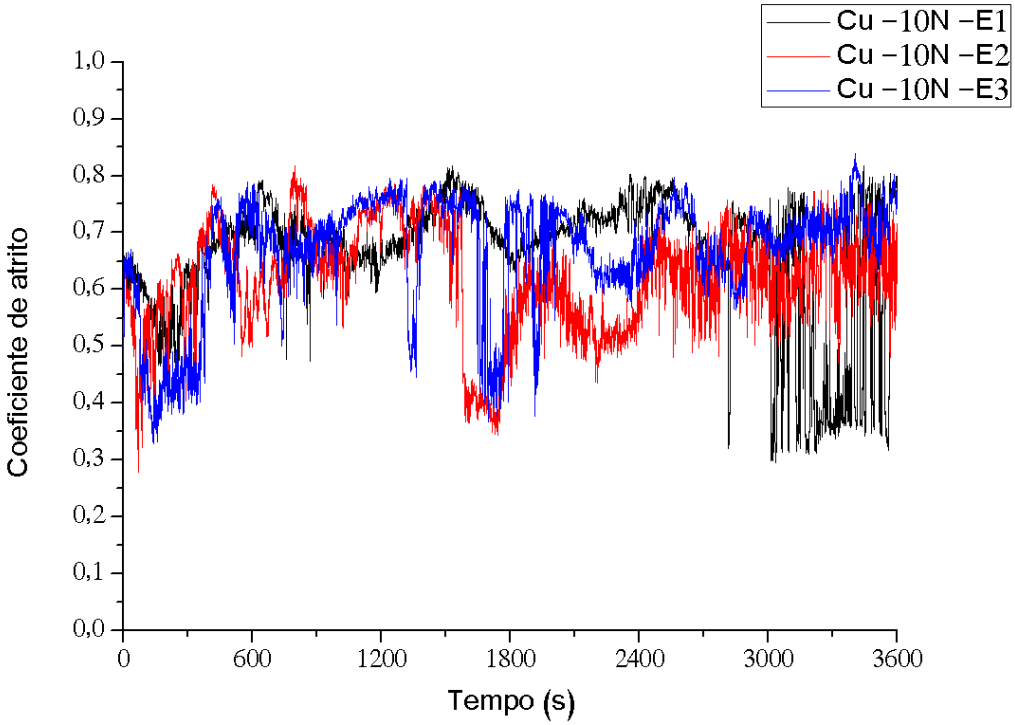

Figure 13: Coefficient of friction vs time(s) chart for copper pins under 0.51 MPa (10N normal load) (Ferreira, 2017).

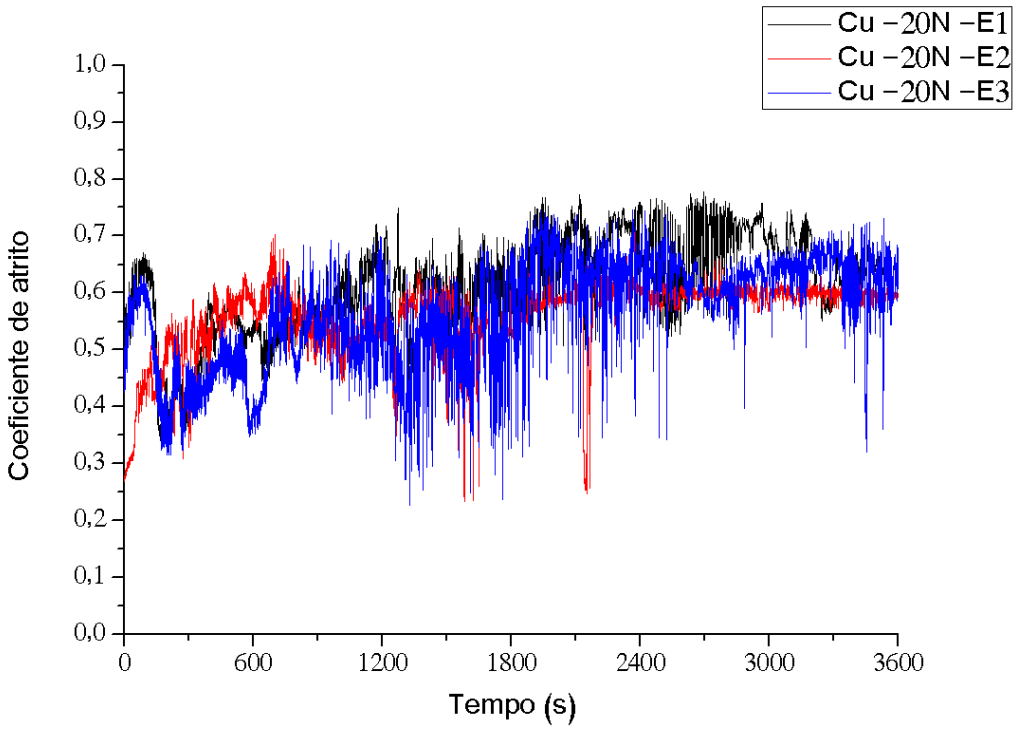

Figure 14: Coefficient of friction vs time (s) chart for copper pins under 1.02 MPa (20N normal load) (Ferreira, 2017).

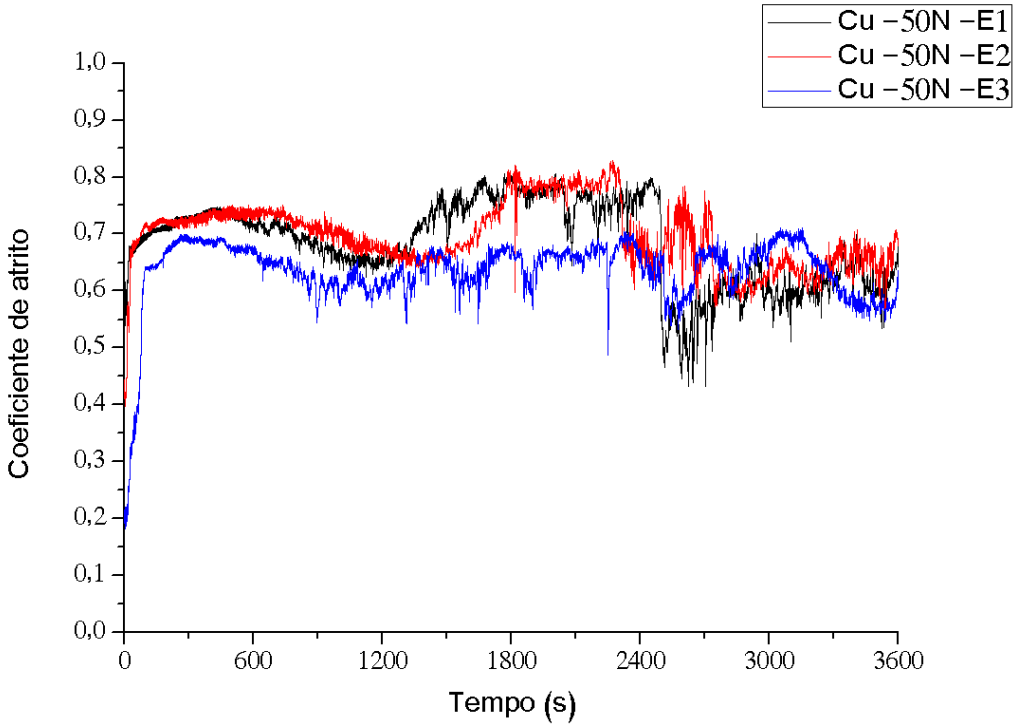

Figure 15: Coefficient of friction vs time chart for copper pins under 2.55 MPa (50N normal load) (Ferreira, 2017).

A graph of the mean values of the coefficient of friction was plotted as a function of the load applied for the tests with copper pins, as shown in (Figure 16). The average CoF decreased from the 0.51 MPa (10N normal load) tribotests to 1.02 MPa (20N normal load) tribotests but increased again in the 2.55 MPa (50N normal load) tribotests for all repetitions.

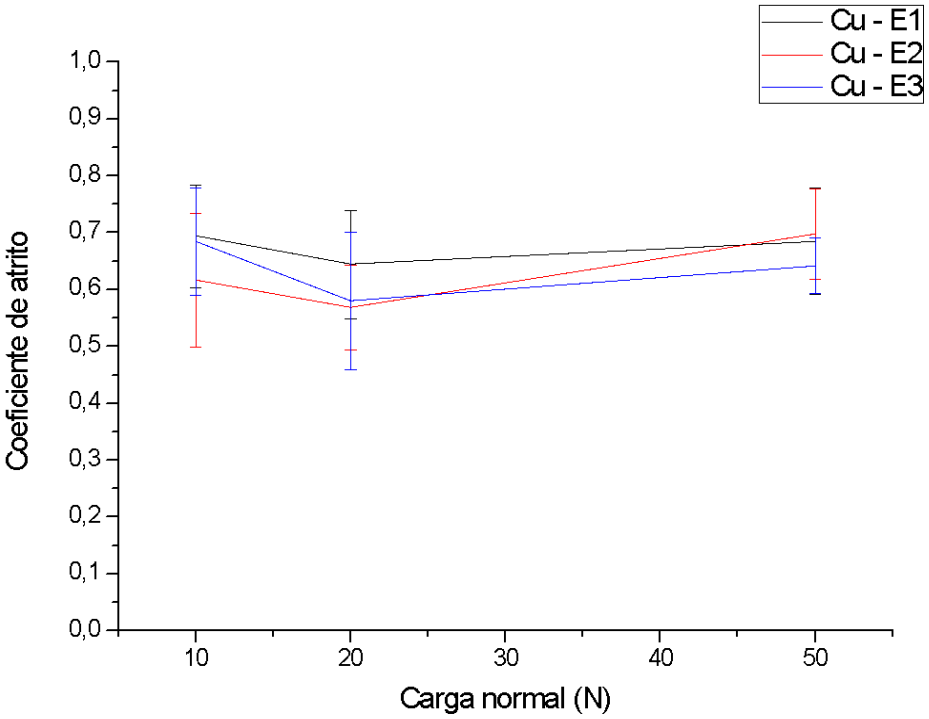

Figure 16: Average coefficient of friction vs normal load chart for copper pins tests. The respective normal pressures are 0.51 MPa (10N normal load); 1.02 MPa (20N normal load) and 2.55 MPa (50N normal load). (Ferreira, 2017).

3.2.2. Aluminium pins

Figures 17, 18 and 19 show the coefficient of friction versus test time for each repetition, using aluminium pins under different normal loads. In comparison to copper tests, CoF values were much more stable. In the test under 2.55 MPa (50N normal load), it is notable that the point coefficient of friction oscillations have increased with the test time, which indicates instability of the coefficient of friction after a considerable slip time. Repetition 2 of the 0.51 MPa (10N normal load) test showed values of the coefficient of friction very far from the pattern of the other repetitions (see Figure 17). The coefficient had a very low value at the beginning of the test (a little more than 0.2) and increased over time until reaching a mean value similar to the other repetitions. However, the point oscillations were much higher compared to repetitions 1 and 3.

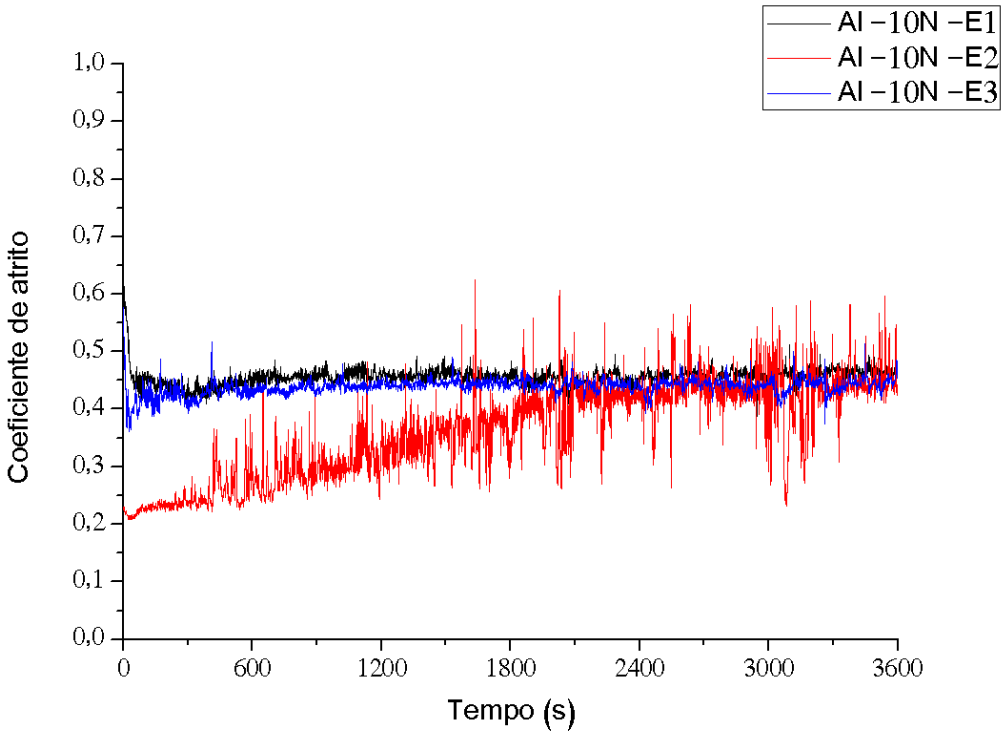

Figure 17: Coefficient of friction vs time (s) chart for aluminium pins under 0.51 MPa (10N normal load).

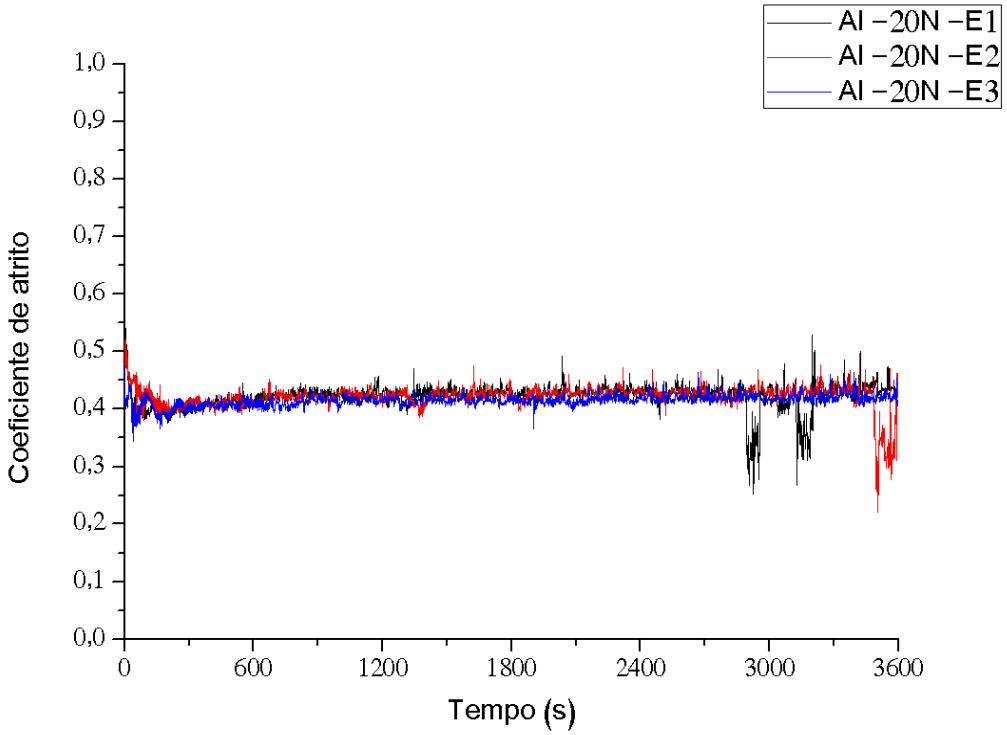

Figure 18: Coefficient of friction vs time (s) chart for aluminium pins under 1.02 MPa (20N normal load) (Ferreira, 2017).

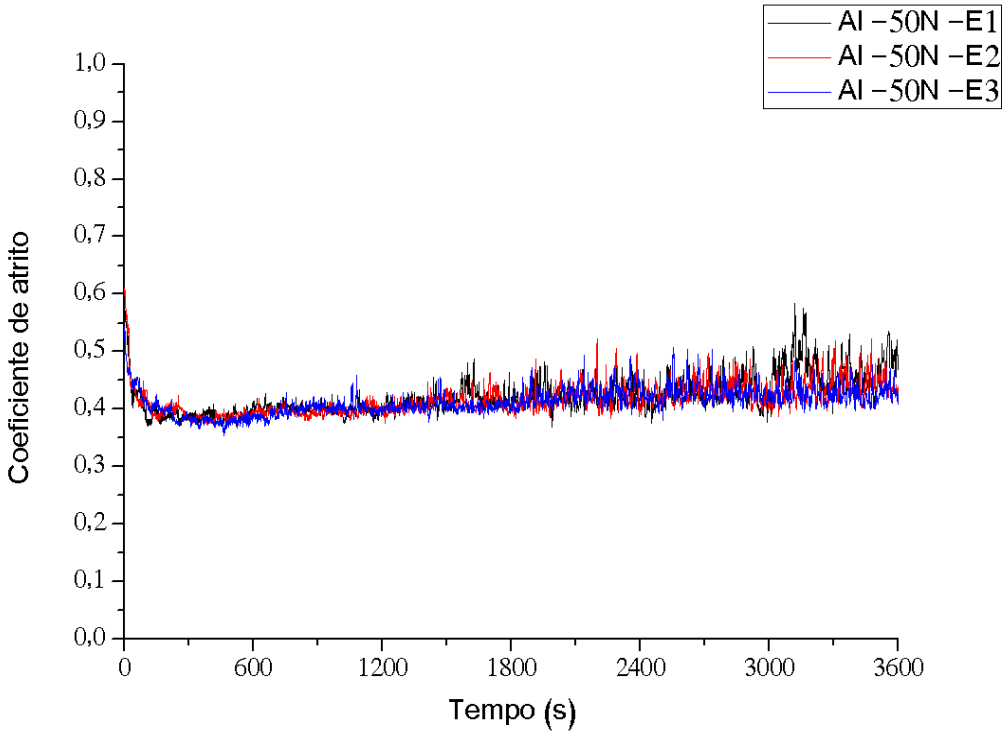

Figure 19: Coefficient of friction vs time (s) chart for aluminium pins under 2.55 MPa (50N normal load) (Ferreira, 2017).

A graph of the mean values of the coefficient of friction was plotted as a function of the load applied for the tests with aluminium pins, as shown in (Figure 20). For all repetitions, excluding repetition 2 of the 0.51 MPa (10N normal load) the average CoF values seems to have decreased as a function of the normal load applied. However, this trend is not statistically proven because of the high standard deviation.

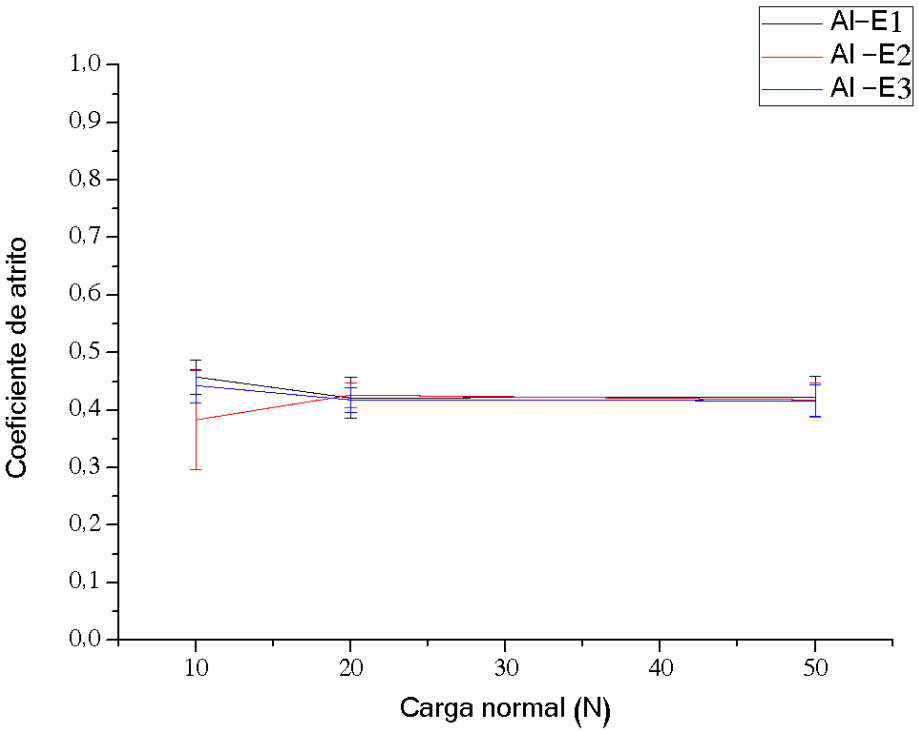

Figure 20: Average coefficient of friction vs normal load chart for aluminium pins tests The respective normal pressures are 0.51 MPa (10N normal load); 1.02 MPa (20N normal load) and 2.55 MPa (50N normal load) (Ferreira, 2017).

3.2.3. Brass pins

Figures 21, 22 and 23 show the coefficient of friction versus test time for each repetition, using brass pins under different normal loads. All repetitions presented a stable curve of CoF. In the 0.51 MPa (10N normal load) tests, the *running-in* phase presented a higher CoF oscillation than the other normal loads. In the test under 2.55 MPa (50N normal load), it is notable that the coefficient of friction oscillations increased with the test time, indicating instability of the coefficient of friction after a considerable slip time. Among the three materials, it was the lowest mean coefficient of friction. Visually, it was also the material that presented greater material detachment (debris with light texture, in the form of “powder”).

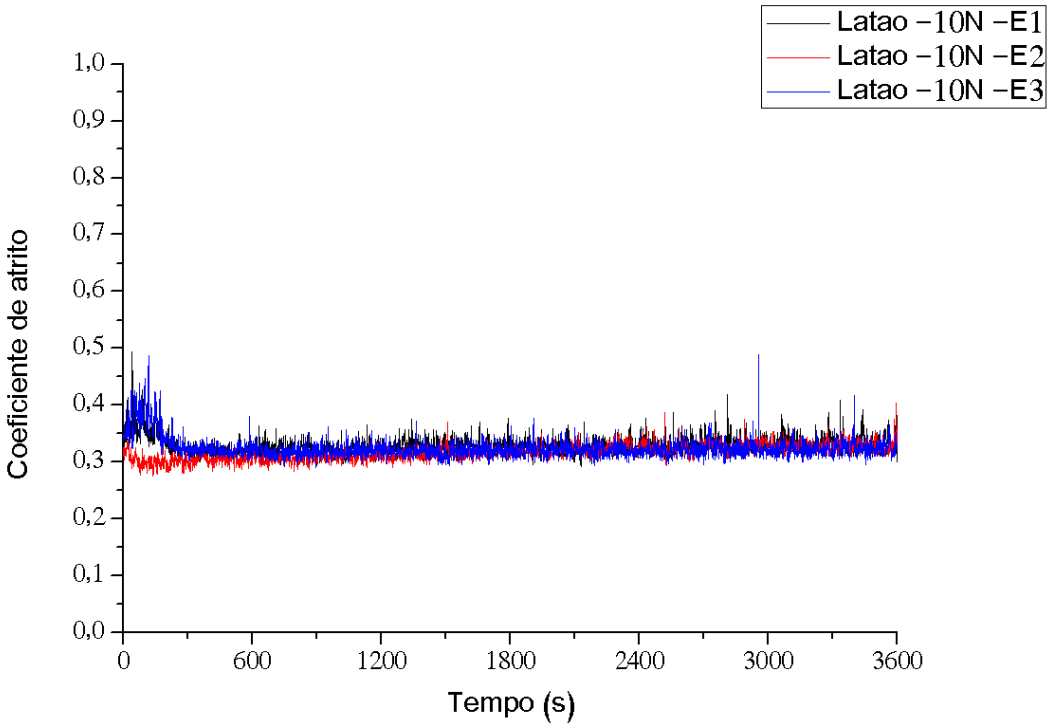

Figure 21: Coefficient of friction vs time (s) chart for brass pins under 0.51 MPa (10N normal load) (Ferreira, 2017).

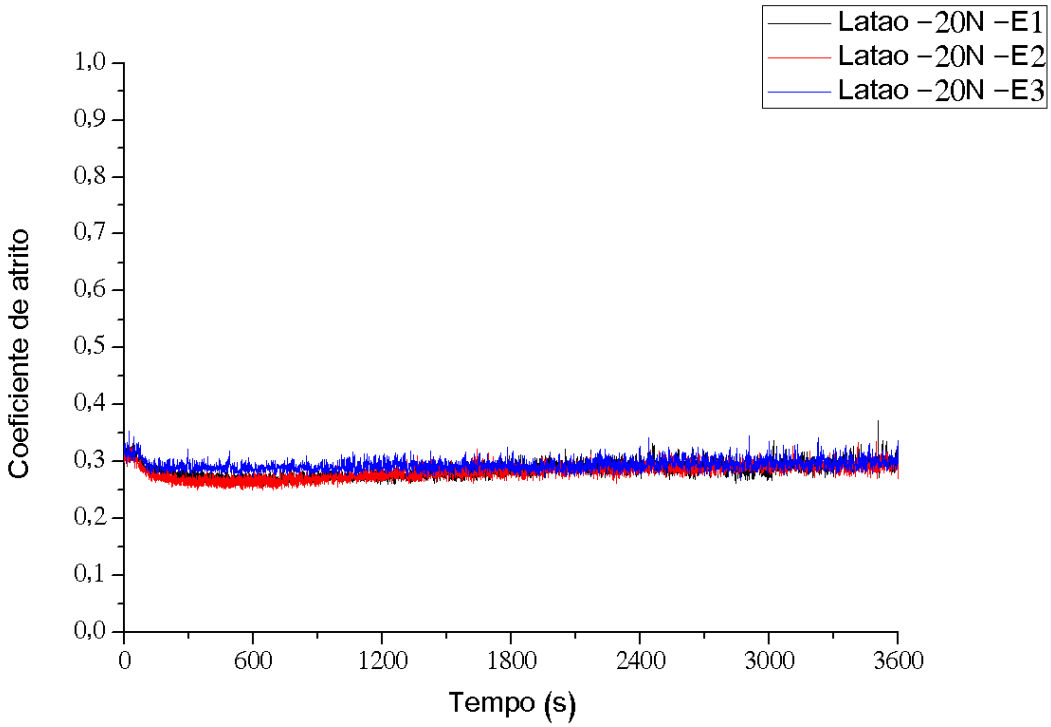

Figure 22: Coefficient of friction vs time (s) chart for brass pins under 1.02 MPa (20N normal load) (Ferreira, 2017).

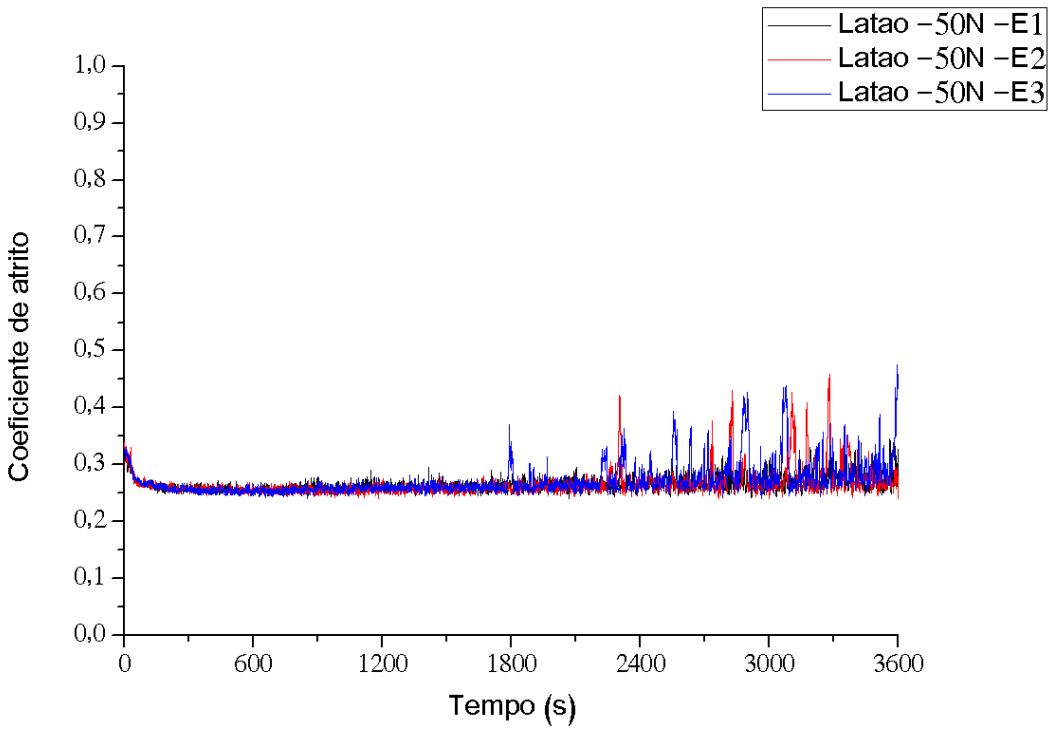

Figure 23: Coefficient of friction vs time (s) chart for brass pins under 2.55 MPa (50N normal load) (Ferreira, 2017).

A graph of the mean values of the coefficient of friction was plotted as a function of the load applied for the tests with brass pins, as shown in (Figure 24). For all repetitions, the average CoF values seems to have decreased as a function of the normal load applied. However, this trend is not statistically proven because of the high standard deviation.

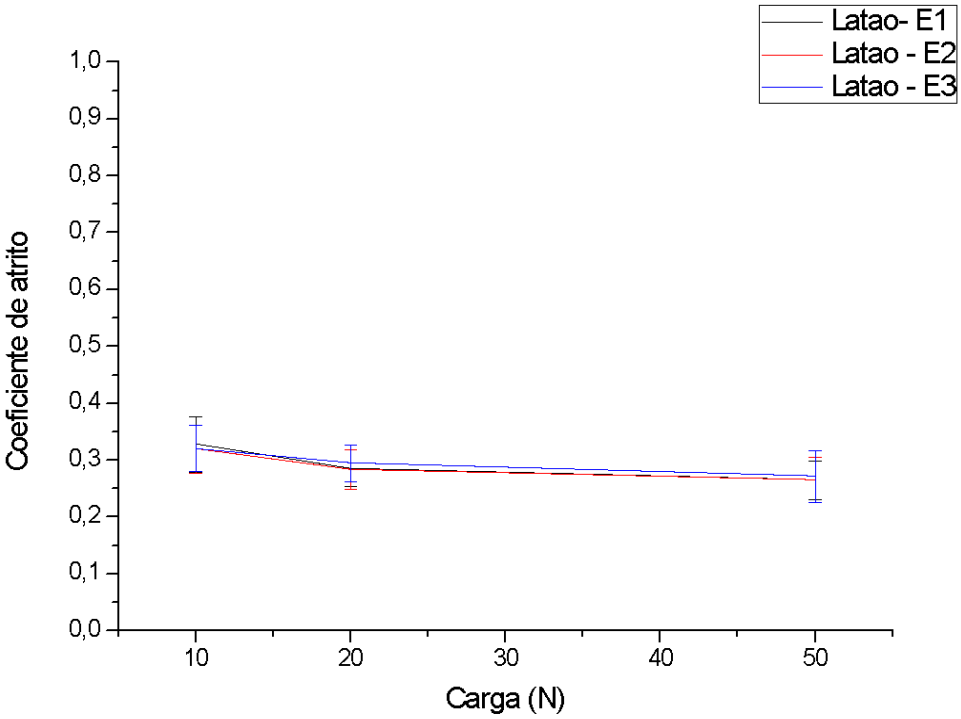

Figure 24: Average coefficient of friction vs normal load chart for brass pins tests The respective normal pressures are 0.51 MPa (10N normal load); 1.02 MPa (20N normal load) and 2.55 MPa (50N normal load) (Ferreira, 2017).

3.3. Consolidated results of the mean coefficients of friction

Table 8 summarises the mean CoF values for all materials and normal load conditions. Among the three materials, copper presented the highest mean coefficient of friction and highest instability, with values around 0.6 to 0.7 for all repetitions. Aluminium and brass presented more stable CoF with lower mean values and standard deviation.

Table 8: Mean coefficients of friction for each pin material and normal pressure.

	Copper	**Aluminium**	**Brass**
0.51 MPa	0.6 – 0.7 *	0.40 ± 0.05 **	0.32 ± 0.05
1.02 MPa	0.6 – 0.7 *	0.40 ± 0.05	0.30 ± 0.03
2.55 MPa	0.6 – 0.7 *	0.40 ± 0.03	0.27 ± 0.03

*Unstable values. For 0.51 MPa: mean point oscillation of 0.3; for 1.02 MPa: mean point oscillation of 0.2; 2.55 MPa: mean point oscillation of 0.05.

**Values obtained for repetitions 1 and 3. Repetition 2 was very unstable and was not considered.

3.4. Microscopic characterisation of steel discs´ tribosurface after tribotesting

The following results are related only to tribotests under 2.55 MPa (50N normal load), because there was no significant discrepancy compared to other loads.

3.4.1. Initial condition of the steel discs' tribosurfaces

Before the tests, the discs were analysed by SE and BSE techniques. The BSE technique shows no phase contrast in the disc surface (Figure 25-b), and the SE technique shows that the surface seemed to be smooth, with little contrast in topography because of grinding lines of the disc (Figure 25-a).

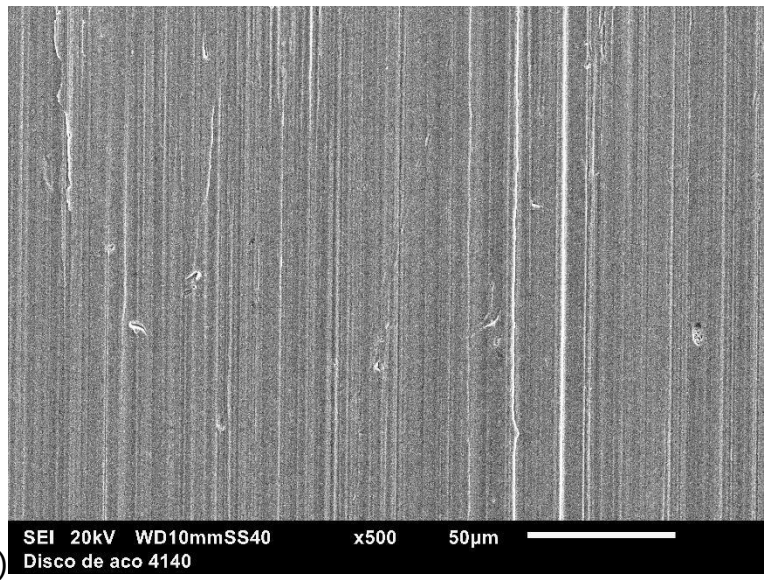

Figure 25: Tribosurfaces of steel discs before tests (500x amplification). a) SEI for topographic contrast. b) BSE image for atomic weight contrast (Ferreira, 2017).

3.4.2. Microscopy and chemical composition for 2.55 MPa tests (copper-steel pair)

The images of the SE and BSE systems (see Figures 26-a,b) show that after the slip, new phases are formed in the wear track of the steel disc due to the atomic and topographic contrasts existing in the analysis. From the maps of the EDS system (see Figures 26-c,d,e), it is noticeable that the regions of these phases coincide with regions that predominate copper and oxygen and insignificant amounts of iron, which leads us to the hypothesis that these regions correspond to copper oxides. Moreover, it is remarkable that some regions correspond to pure copper adhesion (see Figures 26-d).

(a)

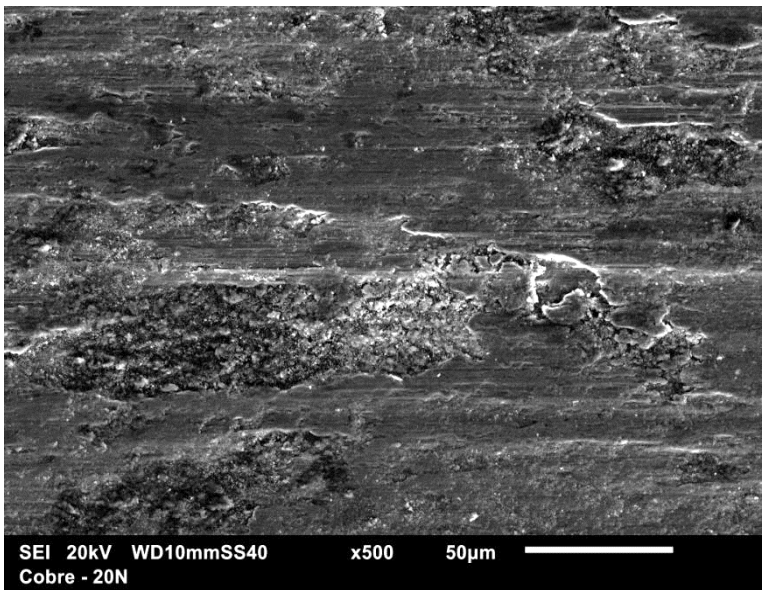

(b)

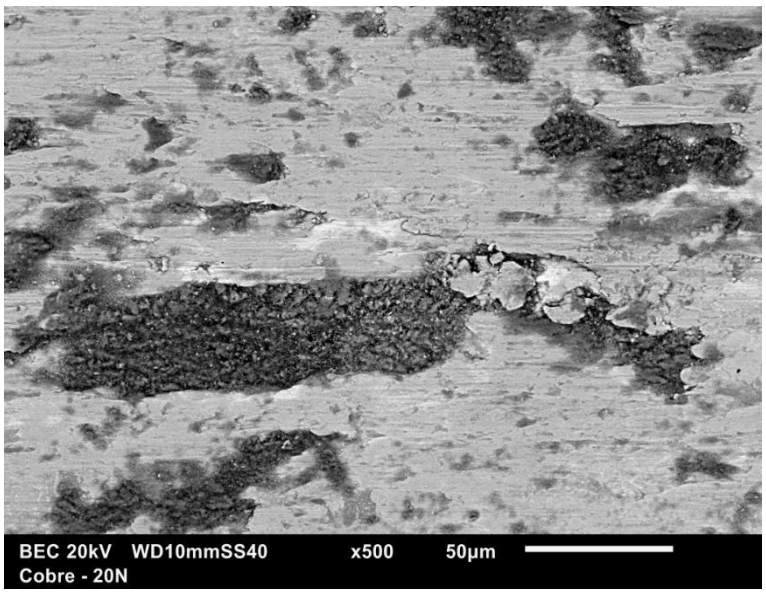

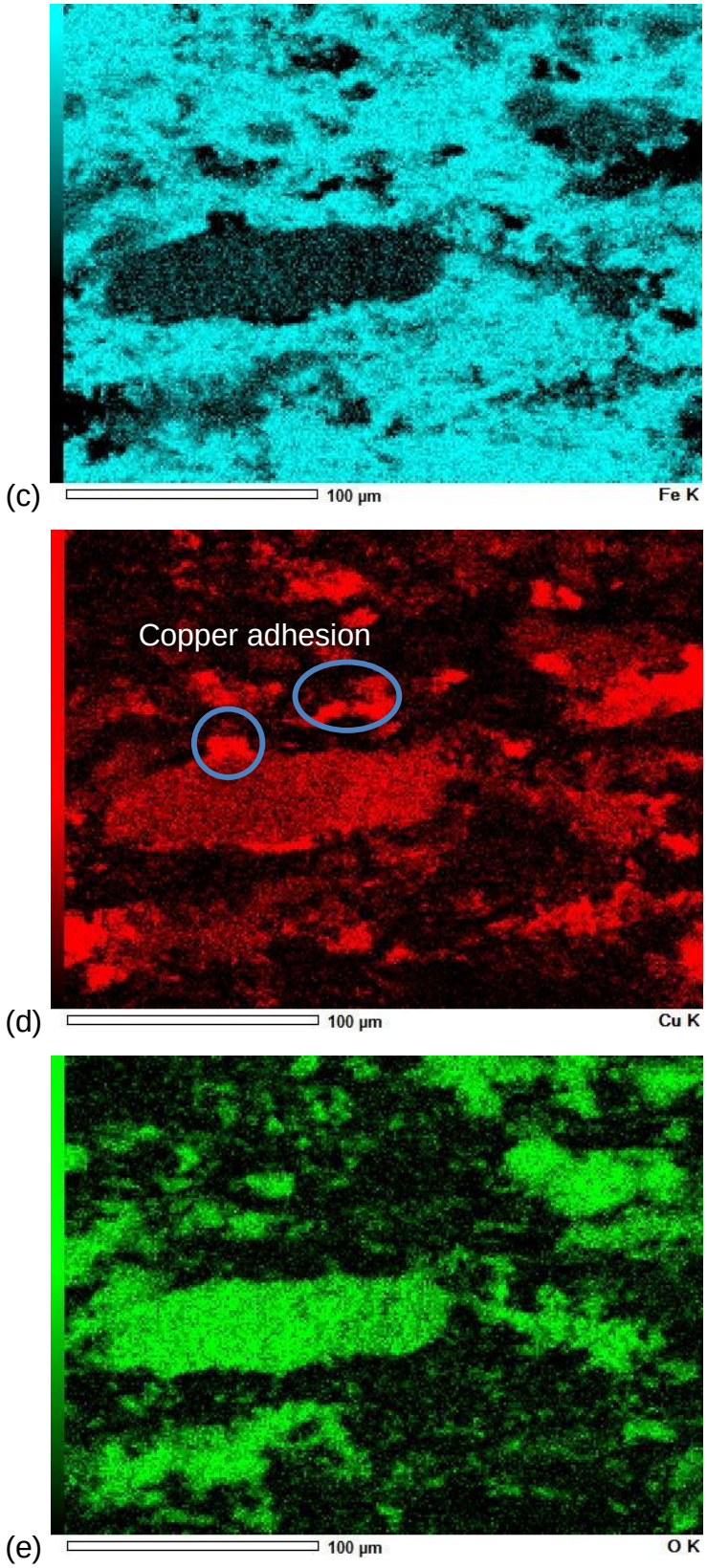

Figure 26: Tribosurfaces of steel discs after tests with copper pins under 2.55 MPa or 50N normal load (500x amplification). a) SE detector image for topographic contrast. b) BSE detector image for atomic weight contrast. c) Composition map for iron. d) Composition map for copper. e) Composition map for oxygen (Ferreira, 2017).

Another observation is that an increase of the normal load increases the concentration of the pin material in the worn trail of the disc, as shown in Figure 27. In that case, the concentration of copper increased, and that of the oxygen decreased.

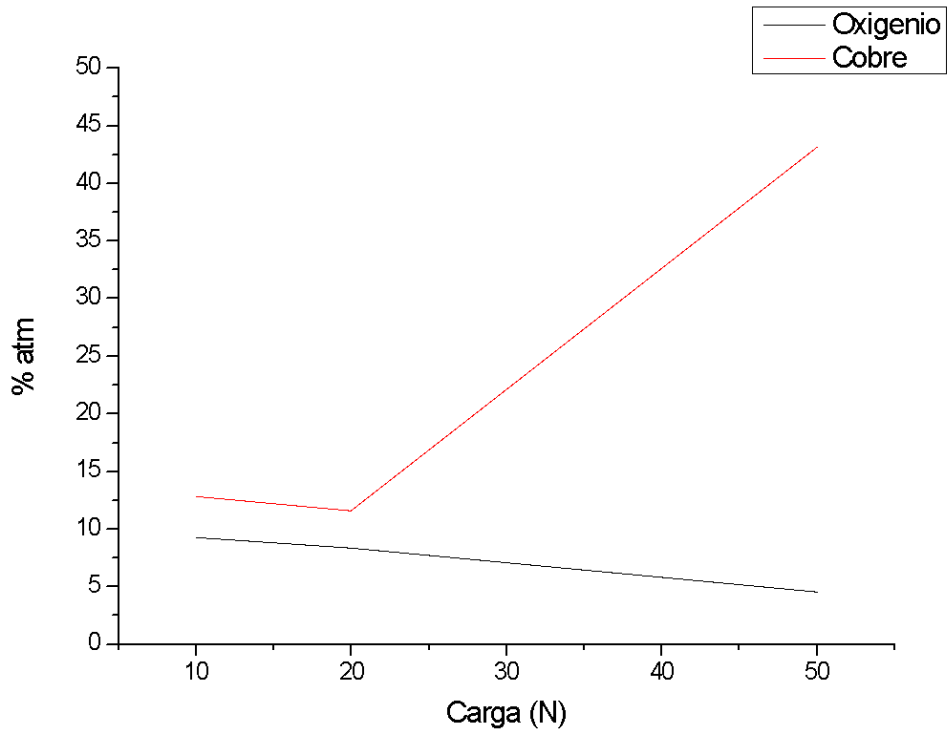

Figure 27: Chart of oxygen and copper atomic composition of the disc tribosurface as a function of normal loads for steel-copper tribopair tests. The respective normal pressures are 0.51 MPa (10N normal load); 1.02 MPa (20N normal load) and 2.55 MPa (50N normal load). Data from EDS analysis under 20 kV tension, 30 min duration and 20% dead time (Ferreira, 2017).

3.4.3. Microscopy and chemical composition for 2.55 MPa tests (aluminium-steel pair)

As in the tests with copper pins, the steel discs tested with aluminium pins may have presented the formation of new phases in the wear track (see Figures 28-a,b). In this case, the regions with these phases coincide with regions of aluminium and oxygen, detected in the EDS elemental mapping (see Figures 28-c,d,e).

(a)

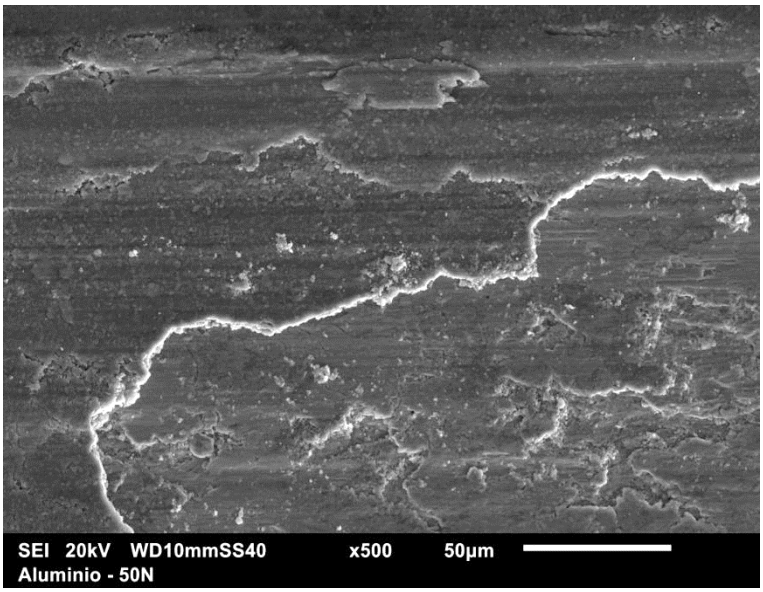

(b)

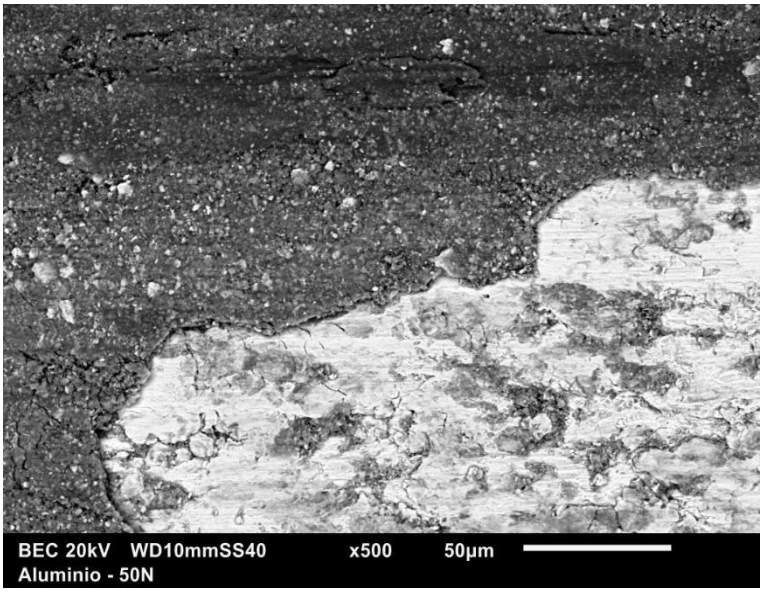

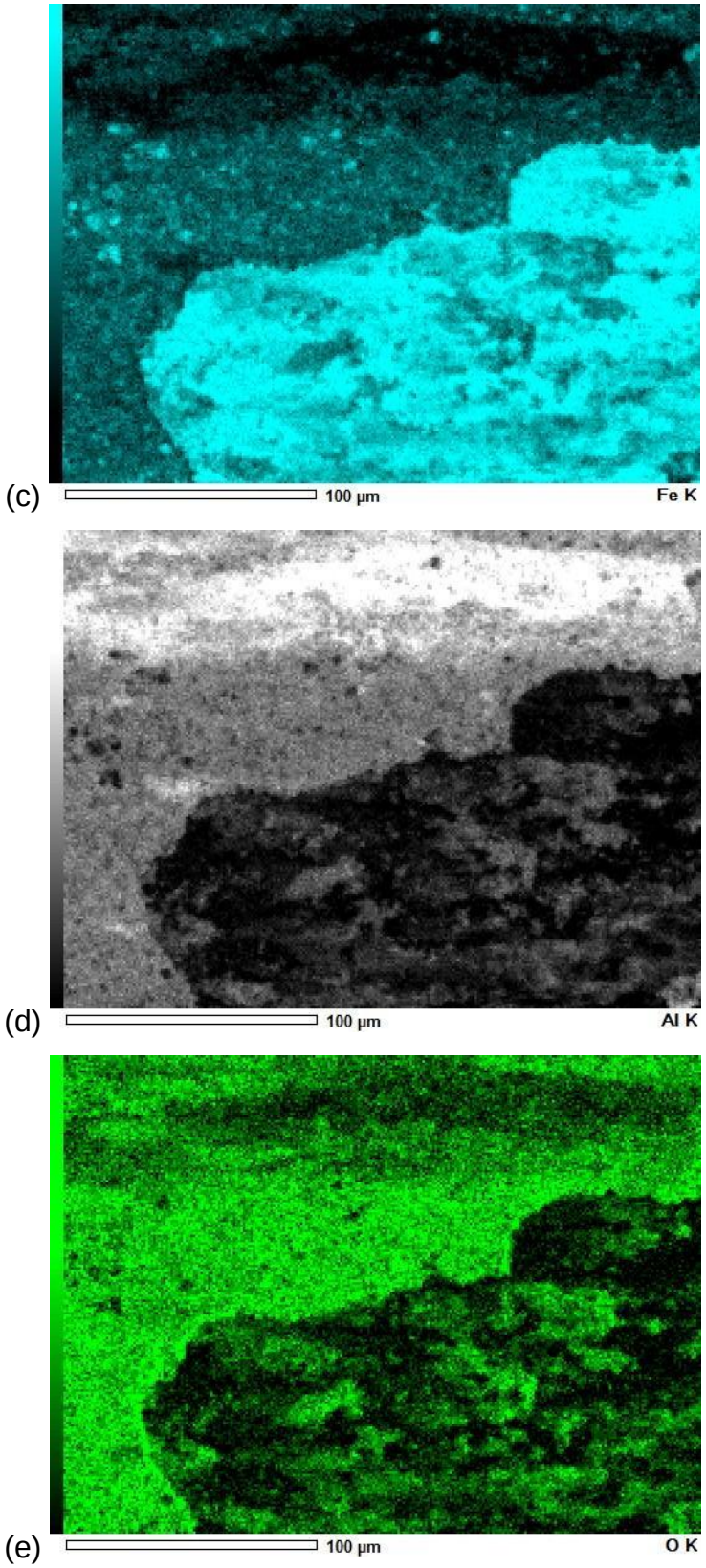

Figure 28: Tribosurfaces of steel discs after tests with aluminium pins under 2.55 MPa or 50N normal load (500x amplification). a) SE detector image for topography contrast. b) BSE detector image for atomic weight contrast. c) Composition map for iron. d) Composition map for aluminium. e) Composition map for oxygen (Ferreira, 2017).

In addition, it is possible to highlight that an increase in normal load did not increase aluminium concentration in the tribosurface of the disc, but rather a small decrease (it remained in the range between 10% and 16%). Oxygen concentration did not change significantly and remained approximately constant between 5% and 7% (Figure 29).

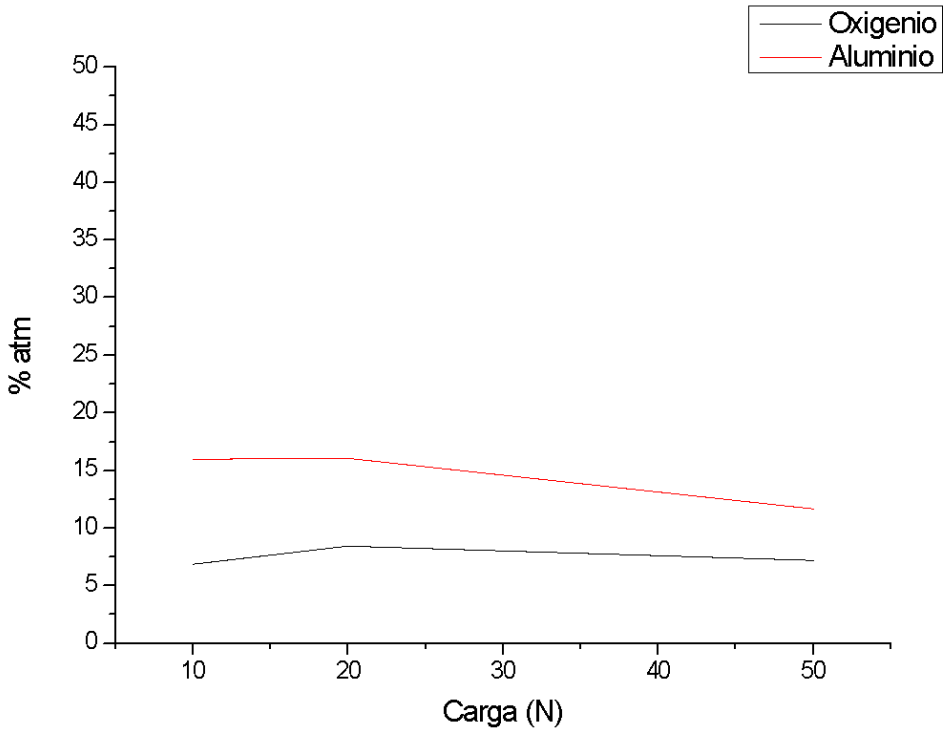

Figure 29: Chart of oxygen and aluminium atomic composition of the disc tribosurface as a function of normal loads for steel-aluminium tribopair tests. The respective normal pressures are 0.51 MPa (10N normal load); 1.02 MPa (20N normal load) and 2.55 MPa (50N normal load). Data from EDS analysis under 20 kV tension, 30 min duration and 20% dead time (Ferreira, 2017).

3.4.4. Microscopy and chemical composition for 2.55 MPa tests (brass-steel pair)

As in the tests with other pins, the steel discs tested with brass pins may have presented the formation of new phases in the wear track (see Figures 30-a,b). In this case, the regions with these phases coincide with regions of copper and zinc detected in the composition map by the EDS system (see Figures 30-c,d,e).

(a)

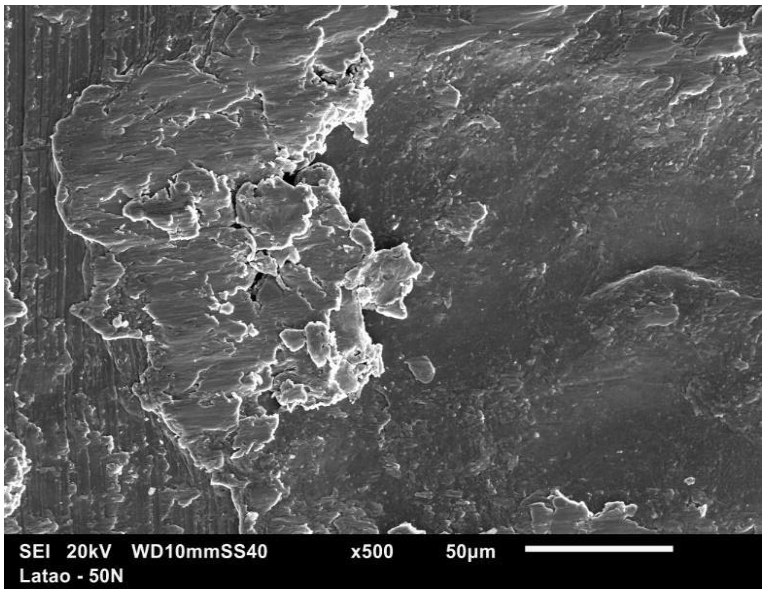

(b)

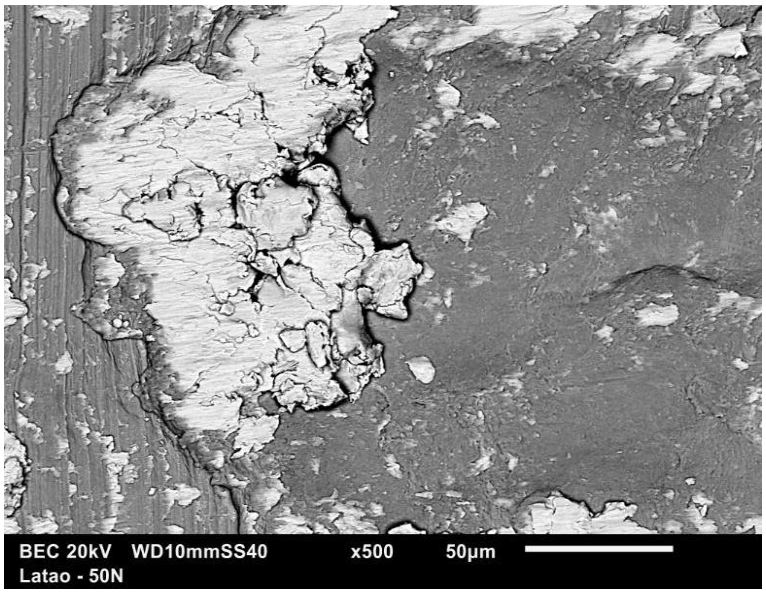

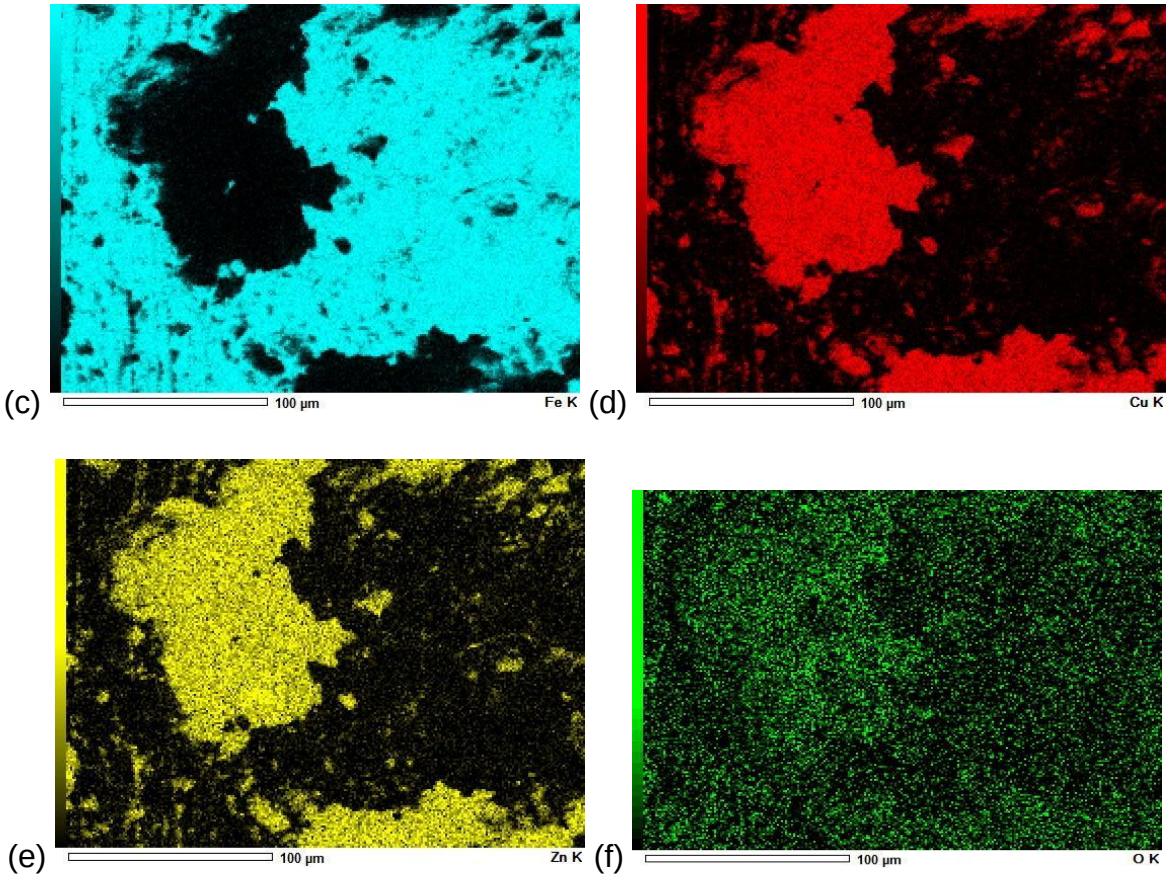

Figure 30: Tribosurfaces of steel discs after tests with brass pins under 2.55 MPa or 50N normal load (500x amplification). a) SE detector image for topographic contrast. b) BSE detector image for atomic weight contrast. c) Composition map for iron. d) Composition map for copper. e) Composition map for zinc. f) Composition map for oxygen (Ferreira, 2017).

There was no significant concentration of oxygen along the region analysed in the wear track of the disc. This can be seen both in the chemical composition maps and in the elementary concentration graph as a function of the normal charge applied (see Figure 31), which shows that the oxygen percentage remained very close to 0% for all tests.

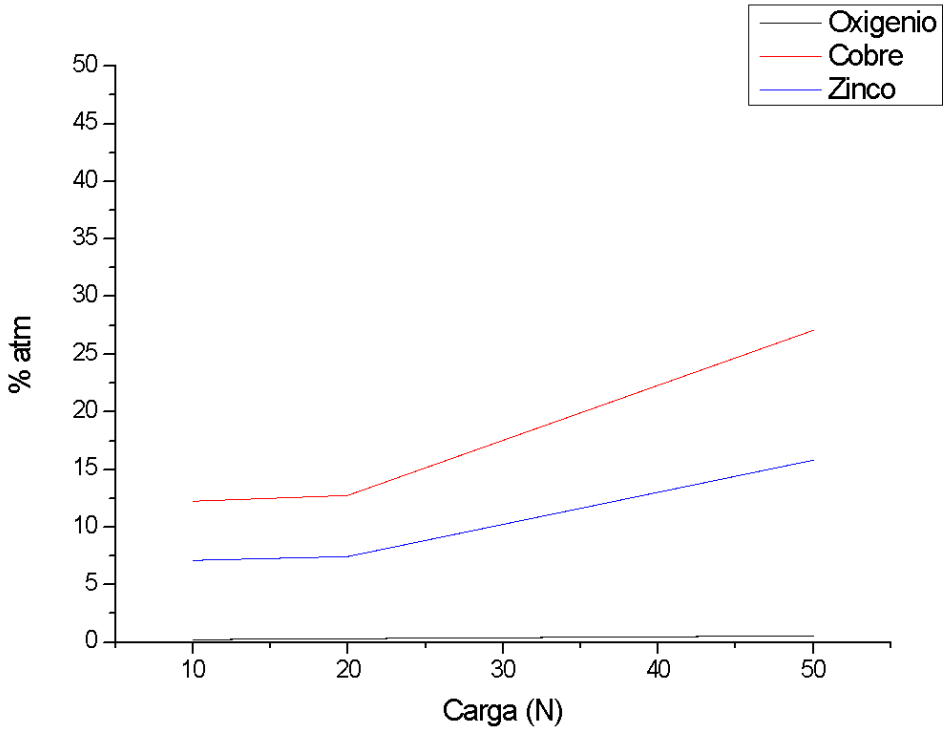

Figure 31: Chart of oxygen, copper and zinc atomic composition of the disc tribosurface as a function of normal loads for steel-brass tribopair tests. The respective normal pressures are 0.51 MPa (10N normal load); 1.02 MPa (20N normal load) and 2.55 MPa (50N normal load). Data from EDS analysis under 20 kV tension, 30 min duration and 20% dead time (Ferreira, 2017).

3.5. Analyses of the disc surfaces in the rugosimeter

3.5.1. Effect of disc grinding on surface analysis

Measurements were made at 4 different points on the disc wear track. In two of them, the grinding lines are parallel to the track, and the other two are perpendicular. It was observed that in the analyses in which the points are parallel to the grinding lines, the 2D profile was impaired, as it became more difficult to perceive which regions the pin went through. An example is shown in Figure 32. For this project, therefore, only results in which grinding lines are perpendicular to the track line are presented, because in that case, it is possible to identify the wear track more clearly.

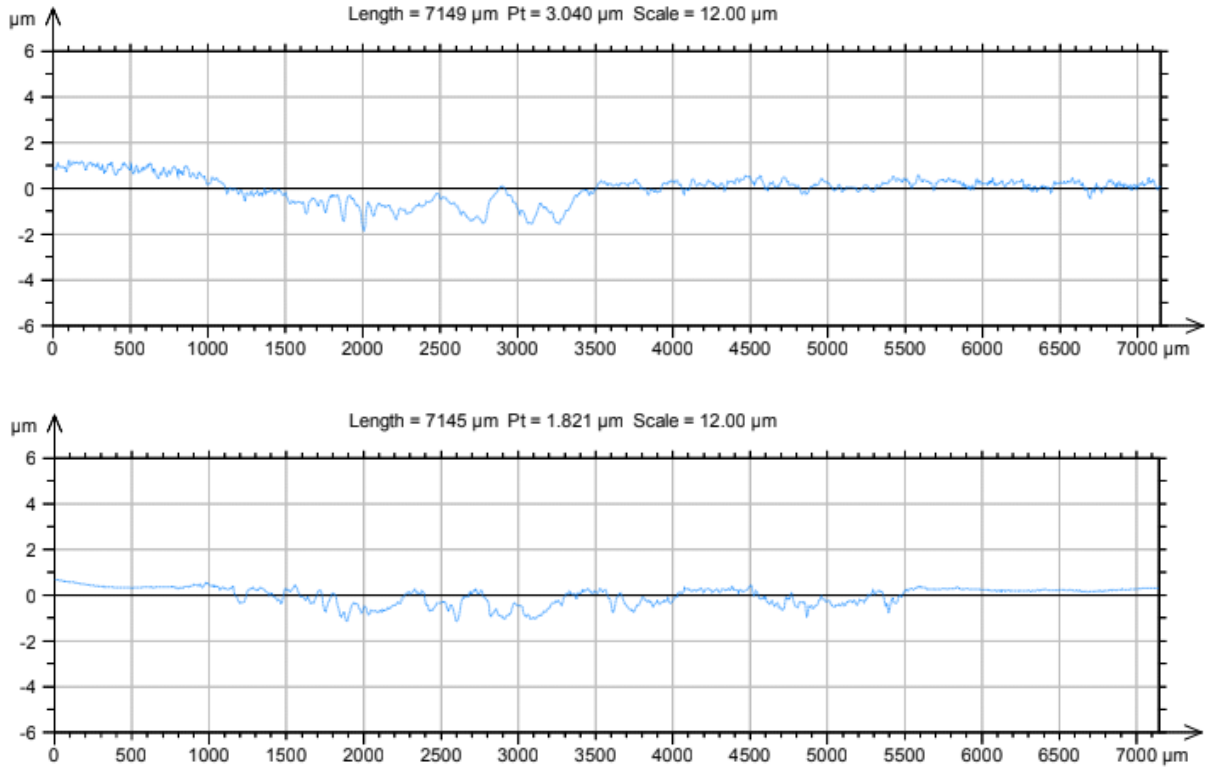

Figure 32: 2D profiles obtained in an analysis in the rugosimeter. The top image represents a point in which the wear line is parallel to the grinding lines, while the bottom figure represents a point in which lines are perpendicular.

3.5.2. Results for tribotests with copper pins (2.55 MPa)

The wear tracks of the discs in the copper-steel tribopair (2.55 MPa or 50N normal load) were analysed in the 3D profilometer (see results in Figure 33). The 2D profile shows the region on which the pin slid. The measured values were 1.023 µm for Sa, 0.0378 µm³/µm² for Vmp and 0.354 µm³/µm² for Vvv.

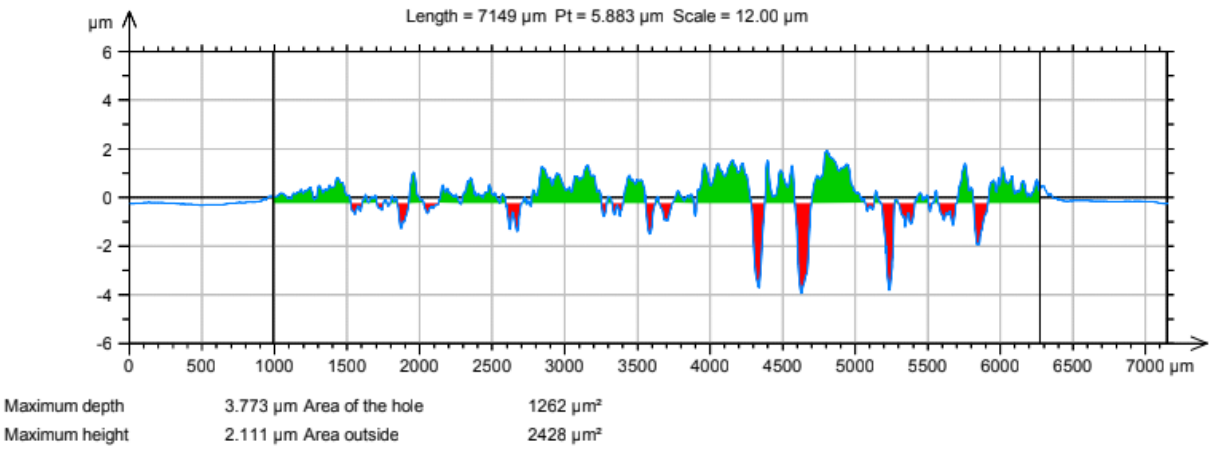

ISO 25178		
Height Parameters		
Sa	1.023	µm
Sq	1.839	µm
Sp	16.71	µm
Sv	24.06	µm
Sku	33.62	
Ssk	-3.971	
Functional Parameters (Volume)		
Vmp	0.03777	µm³/µm²
Vvv	0.3544	µm³/µm²
Functional Parameters (Stratified si		
Sk	2.330	µm
Spk	1.192	µm
Svk	4.645	µm

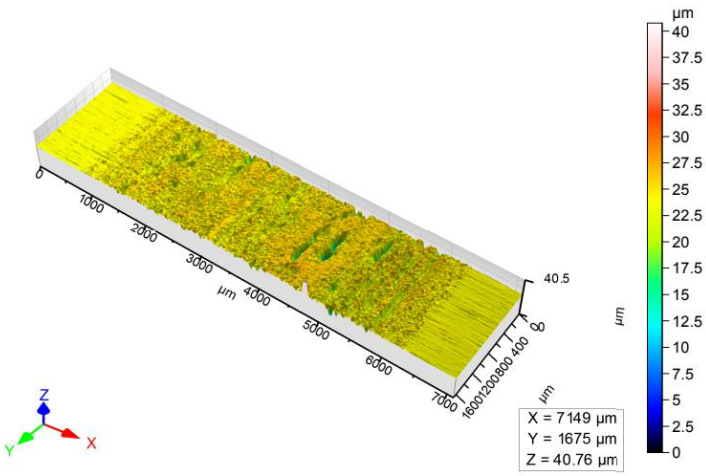

Figure 33: Rugosimeter results for copper pins under 2.55 MPa (50N normal load).

3.5.3. Results for tribotests with aluminium pins (2.55 MPa)

The wear tracks of the discs in the aluminium-steel tribopair (2.55 MPa or 50N normal load) were analysed in the 3D profilometer (see results in Figure 34). The 2D profile shows the region on which the pin slid. The measured values were 0.873 µm for Sa, 0.0810 µm³/µm² for Vmp and 0.186 µm³/µm² for Vvv.

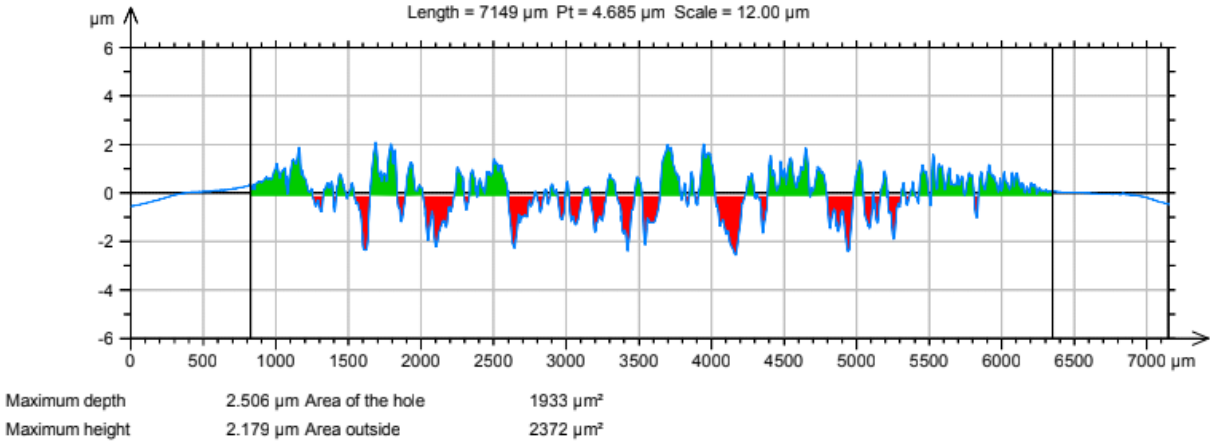

ISO 25178		
Height Parameters		
Sa	0.8673	µm
Sq	1.238	µm
Sp	8.101	µm
Sv	11.30	µm
Sku	6.183	
Ssk	-0.1863	
Functional Parameters (Volume)		
Vmp	0.08105	µm³/µm²
Vvv	0.1895	µm³/µm²
Functional Parameters (Stratified si		
Sk	2.011	µm
Spk	1.474	µm
Svk	1.697	µm

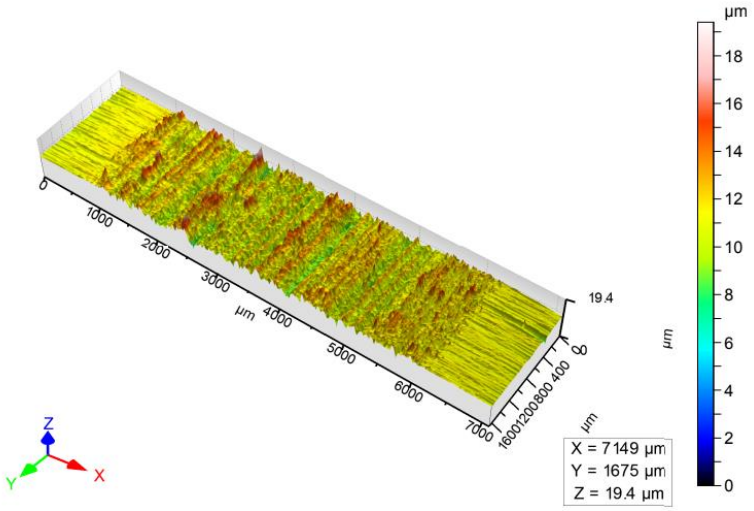

Figure 34: Rugosimeter results for aluminium pins under 2.55 MPa (50N normal load).

3.5.4. Results for tribotests with brass pins (2.55 MPa)

The wear tracks of the discs in the brass-steel tribopair (2.55 MPa or 50N normal load) were analysed in the 3D profilometer (see results in Figure 35). The 2D profile shows the region on which the pin slid. The measured values were 0.954 µm for Sa, 0.264 µm³/µm² for Vmp and 0.164 µm³/µm² for Vvv.

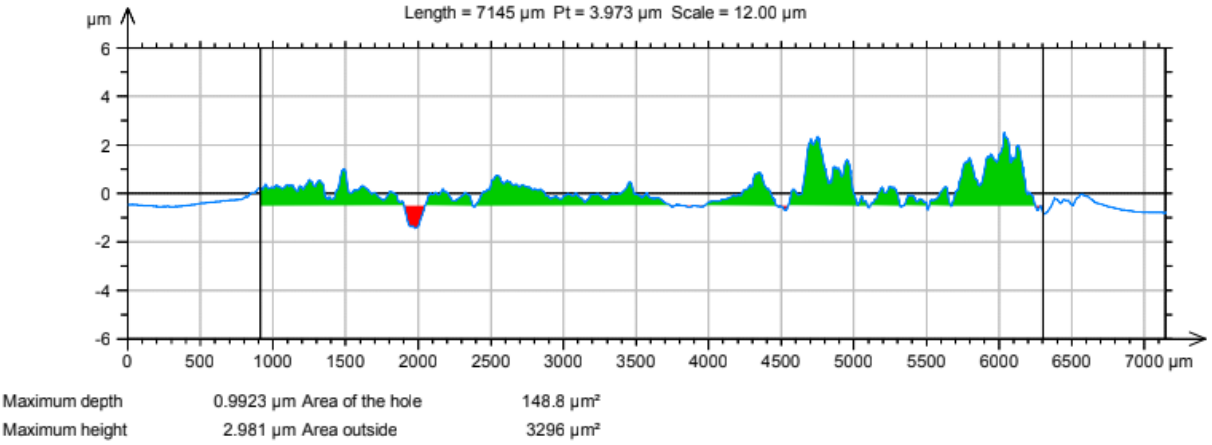

ISO 25178		
Height Parameters		
Sa	0.9537	µm
Sq	1.995	µm
Sp	18.61	µm
Sv	10.39	µm
Sku	33.75	
Ssk	4.402	
Functional Parameters (Volume)		
Vmp	0.2643	µm³/µm²
Vvv	0.1642	µm³/µm²
Functional Parameters (Stratified s		
Sk	1.603	µm
Spk	4.748	µm
Svk	2.390	µm

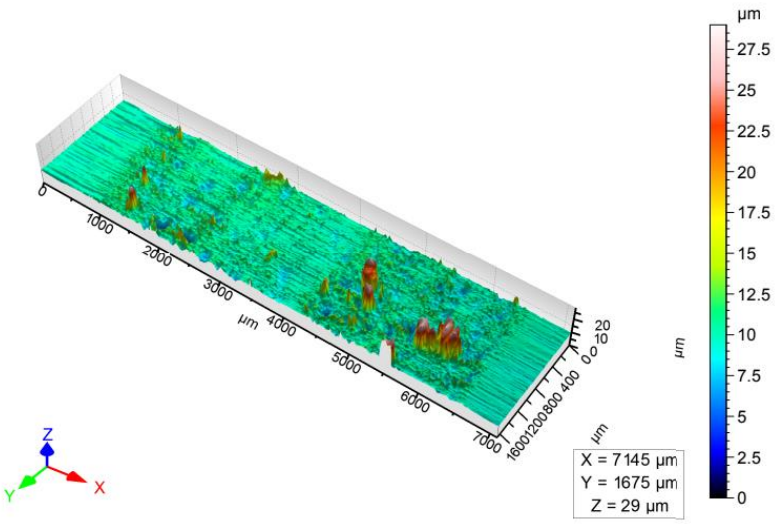

Figure 35: Rugosimeter results for brass pins under 2.55 MPa (50N normal load).

3.5.5. Consolidated results of surface parameters

Table 9 shows the rugosity parameters for each tribopair. Four measures were made for each tribopair: two in a perpendicular direction to the grinding lines and the other two in a parallel direction to the grinding lines. The mean values for these two types of measures, so the mean value for all 4 measures were calculated and summarised in Table 10.

Table 9: 2D and 3D rugosity parameters obtained for 2.55 MPa (50N normal load), in perpendicular and parallel directions, for aluminium, copper and brass pins. Two different points were analysed.

Parameters (2.55 MPa)		**Direction of grinding lines in relation to the wear track**			
		Perpendicular		Parallel	
Aluminium	Sa	0.867	1.171	1.132	0.980
	Vvv	0.190	0.223	0.235	0.221
	Vmp	0.081	0.063	0.122	0.090
Copper	Sa	1.023	0.867	1.139	1.075
	Vvv	0.354	0.341	0.356	0.347
	Vmp	0.038	0.033	0.045	0.050
Brass	Sa	0.954	0.909	0.881	0.993
	Vvv	0.164	0.148	0.116	0.184
	Vmp	0.264	0.185	0.160	0.128

.

Table 10: Mean of rugosity parameters obtained for 2.55 MPa (50N normal load), in perpendicular and parallel directions, for aluminium, copper, and brass pins. Also, a column with the total mean was added.

Parameters (2,55 MPa)		**Perpendicular (Mean values)**	**Parallel (Mean values)**	**Total (Mean values)**
Aluminium	Sa	1.0191	1.0559	1.0375
	Vvv	0.2061	0.2282	0.2171
	Vmp	0.0720	0.1059	0.0889
Copper	Sa	0.0945	1.1070	1.0260
	Vvv	0.3479	0.3516	0.3498
	Vmp	0.0356	0.0472	0.0414
Brass	Sa	0.9314	0.9368	0.9341
	Vvv	0.1560	0.1502	0.1531
	Vmp	0.2244	0.1442	0.1843

Figures 36, 37 and 38 show the mean values of Sa, Vmp and Vvv (respectively) as a function of the normal load for each tribopair tested. It is noticeable that for all tribopairs, the increase of the normal load provoked an increase in the three rugosity parameters. Aluminium presented the highest values of Sa for all normal loads. For

the 2.55 MPa (50N normal load) tests, the brass-steel tribopair presented the highest Vmp value, and the copper-steel tribopair presented the highest Vvv value.

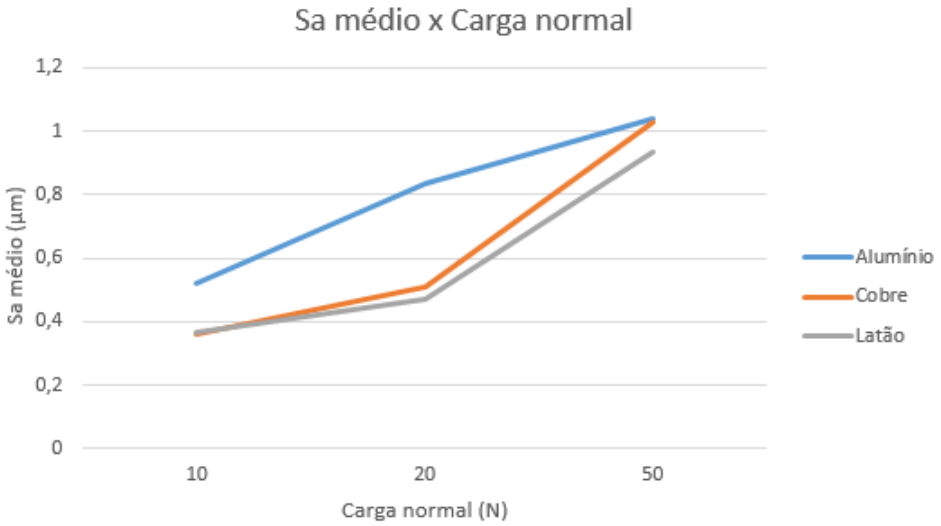

Figure 36: Chart of mean Sa as a function of normal loads for each tribopair (aluminium in blue, copper in orange and brass in grey). The respective normal pressures are 0.51 MPa (10N normal load); 1.02 MPa (20N normal load) and 2.55 MPa (50N normal load).

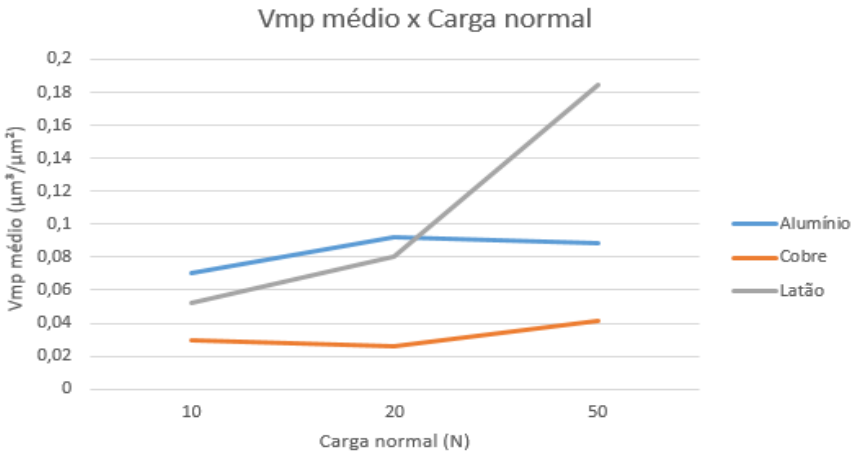

.

Figure 37: Chart of mean Vmp in the function of normal loads for each tribopair (aluminium in blue, copper in orange and brass in grey). The respective normal pressures are 0.51 MPa (10N normal load); 1.02 MPa (20N normal load) and 2.55 MPa (50N normal load).

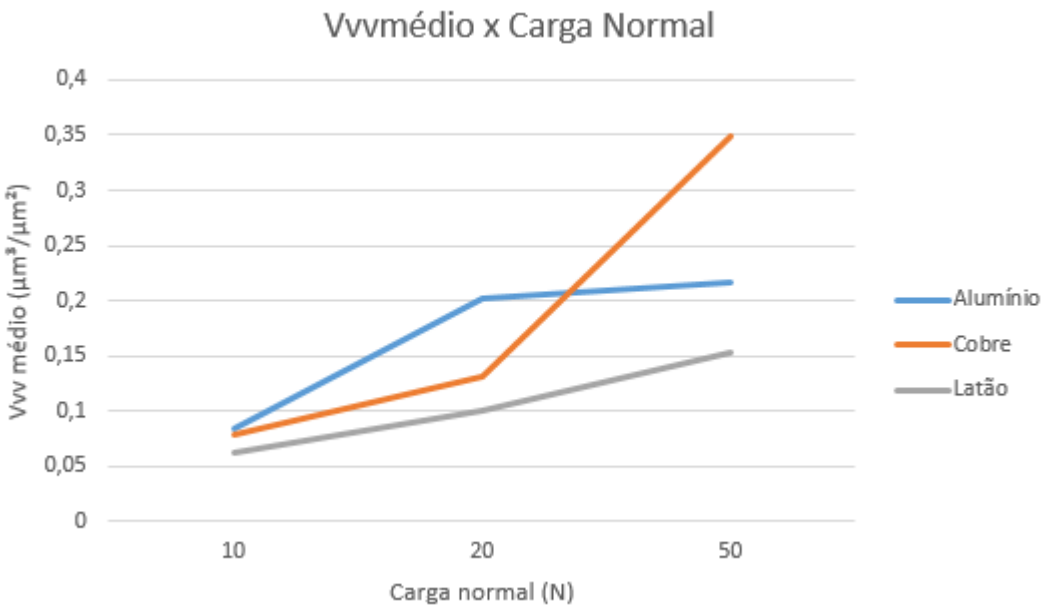

Figure 38: Chart of mean Vvv as a function of normal loads for each tribopair (aluminium in blue, copper in orange and brass in grey). The respective normal pressures are 0.51 MPa (10N normal load); 1.02 MPa (20N normal load) and 2.55 MPa (50N normal load)

4. DISCUSSION

4.1.1. Coefficient of friction

For all tribopairs, the increase of the normal load applied led to a decrease in the mean friction coefficient. However, this is not statistically proven because of the high standard deviation presented in each condition. Chowdury et al. (Chowdhury, Khalil, Nuruzzaman, & Rahaman, 2011) evaluated the behaviour of a stainless steel pin against an aluminium disc under 10N normal load pin versus disc tribological test, varying the test rotation between 500 and 2500 rpm (Figure 39). The authors verified that the increase of the normal load and the sliding speed decreased the coefficient of friction.

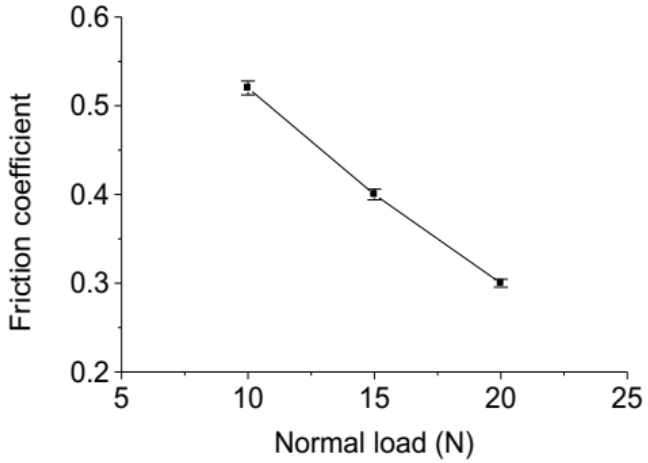

Figure 39: Evolution of the coefficient of friction in the tribological pin versus disc test in aluminium-steel tribological pair with a normal load of 10N and relative humidity of 70%. (Chowdhury et al., 2011)

Additionally, Samad et al. studied the wear behaviour of copper alloy (CuZn39Pb2) and aluminium (AA7075) pins against cast iron GG25 (Samad et al., 2020). Despite the slight difference in the materials' composition, similar results were observed. The influence of initial surface roughness on the coefficient of friction was observed to be more significant for copper alloy tests than for aluminium tests, which can also be seen in the results of this project. A comparative case study between an industrial setup and a lab setup shall help develop a better understanding of the wear behaviour of materials by linking field conditions with that of the conditions in a laboratory. Moreover, results from an industrial setup can provide prototypes for solving industrial problems.

Bouchoucha et al. (Bouchoucha, 1995) compared the sliding behaviour of a copper pin against steel in different atmosphere conditions. When an electric current was applied to prevent oxide formation, it was observed that the CoF behaviour was very unstable with metal adhesion to the steel's surface. Theses results could help to expalin the instability of copper's CoF observed in the present project: as the EDS results showed, there was metal adhesion only to the disk of the copper-steel tribopair.

Regarding the brass-steel tribopair, similar behaviour of decreasing coefficient of friction with increased load was reported in the literature (Pereira, 2014). Furthermore, Chowdury (Chowdhury et al., 2011) stated that the coefficient of friction might not remain constant as a function of the normal load, and the increase of this load may increase the surface roughness and the amount of test debris, which may decrease the coefficient of friction. This is coherent with the results of the current project because the brass-steel tribopair was the one that presented the lowest CoF and the higher quantity of debris.

A hypothesis for the instability of the coefficient of friction of copper could be the continuous formation and defragmentation of the tribolfim, making its behaviour very unstable. However, further studies should be conducted to validate this hypothesis.

4.1.2. Mass variation of pins

Table 11 shows the mean losses of mass of the pins after the test. Comparing the variation of the average mass of the pins, it is possible to highlight a similarity between the tribotests. It was noticed a trend of increasing the average mass loss of the pins as a function of the normal load applied. However, it is very remarkable that the brass pin was the one that wore the most for the three normal loads, losing up to 0.278 g on average when tested under 2.55 MPa (50N normal load), whereas the other pins lost 0.014g (copper) and 0.011g (aluminium), which are more similar values. It is noticeable that a significant amount of debris was observed in the brass tribotests (in powder form), which confirms the results obtained in Table 11. Moreover, the formation of an opaque tribofilm was observed on the disc. These results are coherent with the findings of Chowdury (Chowdhury et al., 2011), in which the increase of the normal load provoked an increase of the tested debris.

Table 11: Mean mass losses for each pin material and normal load.

Normal pressure	Copper	Aluminium	Brass
0.51 MPa	(0.002) g	(0.004 ± 0.001) g	(0.047 ± 0.001) g
1.02 MPa	(0.004) g	(0.007) g	(0.098 ± 0.005) g
2.55 MPa	(0.014 ± 0.003) g	(0.011) g	(0.246 ± 0.001) g

4.1.3. Tribological behaviour

According to Kato (Kato, 2007), when metals slide one against the other in an environment with air, there may be a sliding transition from severe to mild, in which there is a lower wear rate. Thus debris arising from wear plays an essential role in establishing wear in the *mild* type because it is shown that protective layers are produced during the mild wear by compacting and sintering oxidised debris between the sliding surfaces and that these formed layers would cause a decrease in friction and wear because of that adhesion. Figures 40 and 41 show the curve “total volume from wear versus diffusion coefficient of oxides” and the curve of “total volume from wear versus slip distance”, respectively, obtained by Kato (Kato, 2007) when injecting nanoparticles of oxides between sliding metal surfaces.

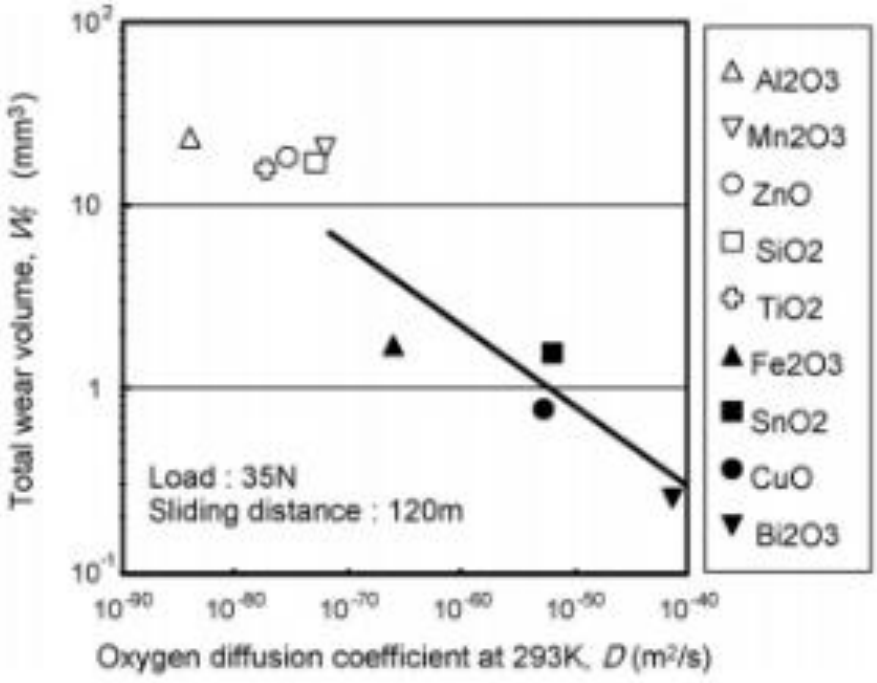

Figure 40: Plots of total material wear volume versus oxygen diffusion coefficient at 293K temperature for different oxides. (Kato, 2007)

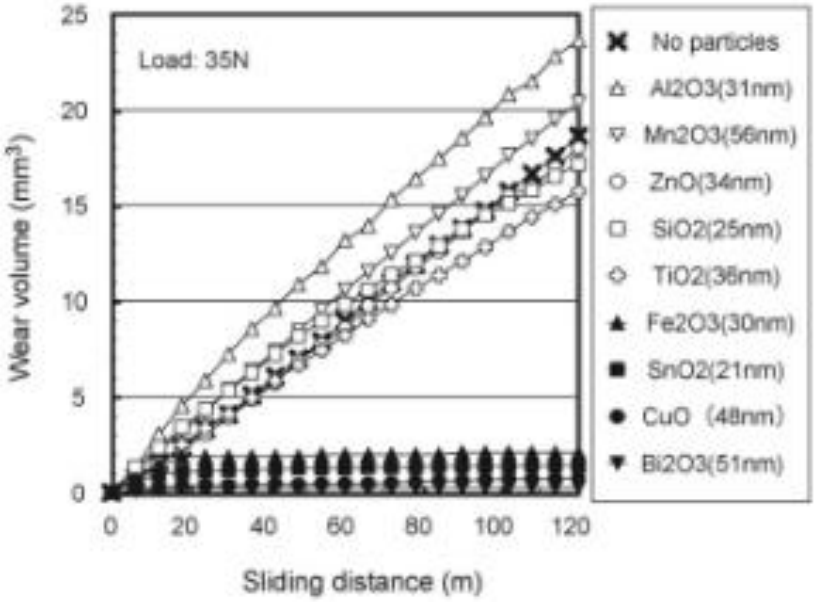

Figure 41: Plots of total material wear volume versus sliding distance for different oxides under 35N normal load. (Kato, 2007)

Based on these curves, it can be concluded that when zinc oxides and aluminium particles (low oxygen diffusion coefficient) have been injected, no transition from severe wear to mild wear was identified because the rate of wear by distance did not remain constant. Differently, the copper oxide (high coefficient of oxygen diffusion) presented a constant wear volume after the “running-in” stage, which would be the initial phase of the slip before the transition to the “Mild” regime occurred. It should be noted that the higher the oxygen diffusivity in the oxide, the lower is the total wear volume obtained.

This suggests that slips with the formation of copper oxide as the third body can lead to the formation of a protective film, as there would be a higher rate of formation of tribofilm due to sintering of oxidised particles, resulting in a lower amount of wear, unlike to what happens to aluminium. The above hypothesis may be reinforced by the fact that the pins of brass and aluminium presented a more significant loss of mass than the pins of copper. In addition, by graphs of attachment of pin material as a function of the load obtained by the SEM, it is noted that although the change in pin mass was lower for copper, the copper adhesion to the disc was higher than the tests with aluminium and brass, which also suggests the formation of protective tribofilm. These results are compatible with the findings of other projects. Rodrigues conducted PoD tribotests (steel/steel pair) with the addition of copper particles as an interfacial media and varied their granulometry (Rodrigues, 2016). The researcher found that this

addition contributed to the increase of average CoF of the system compared to the system without the addition of interfacial media, and the highest values for the friction coefficient were obtained for the finer Cu particle granulometry. Moreover, the addition of copper powder to the test was able to form a transfer layer with the presence of oxygen, as showed by EDS, suggesting that there was the formation of oxide third body with a protective behaviour.

In other studies, the same researcher compared the results of pure copper addition in PoD steel/steel tribotests to the results of magnetite, graphite and zirconia additions. Rodrigues studied the tribological behaviours when these additions were made separately and mixed in different testing conditions (temperature, granulometry, interfacial media, composition, etc.) (Rodrigues, 2017; Rodrigues, 2015). Separately, graphite and magnetite additions decreased the friction coefficient compared to copper addition. When mixed, the results of the coefficient of friction varied significantly according to the testing conditions, showing that in a more complex system with many variables involved, it becomes hard to predict its tribological behaviour.

Finally, according to the graphs obtained by the rugosimeter results, the mean disc roughness (Sa parameter) after aluminium tests was higher for all loads, suggesting that the particles formed present a more abrasive behaviour, in concordance with the finding of Kato (Kato, 2007), where aluminium presented a severe tribological behaviour. The results obtained for Vvv and Vmp were inconsistent, with the need to perform more tests and analyses.

4.1.4. Final remarks, the future of copper-free brake pads

Although copper-free formulations are already available in the market (Bosch, 2021; Fras-le 2021; Hella-Pagid, 2021), researchers have made many efforts to replace copper with other constituents. A study conducted by the University of Trento (Leonardi, 2020) aimed to develop, produce and test new formulations for brake pads without copper, comparing them to current market products. It is found that in 2018, the Cu-free brake pads surpassed 50% of all granted certifications, and satisfactory results have been achieved. However, based on its state-of-the-art findings, none claimed success so far to achieve a complete Cu-free formulation efficient as Cu-full formulations. Also, it is not clear yet whether the market copper-free formulations do not create other environmental impacts. In their study, a Cu-free formulation with a combination of steel fibres and barite displayed an improved wear behaviour and a stable coefficient of friction compared to a reference market Cu-full master-batch. New formulations were developed varying several constituents of a brake-pad apart from copper and then ranked based on performance and emissions. Further, the best material was tested on a real car.

Other researchers have also been studying alternative materials for copper-free brake pads (Bhatt et al., 2021; Kalel et al., 2021; Tavangar et al.; 2020; Aranganathan et al., 2015; Mahale, 2019; Hu, 2016). A few of these studied formulations are summarised in Table 12 (non-exhaustive list). It is noticeable that information concerning market-released formulations was not fully disclosed. On the other hand, research-level formulations presented further details about their compositions. Thermo-graphite, aluminium alloys, and stainless steel were the most mentioned materials to replace copper, but each study presented its composition and testing conditions.

Table 12: Non-exhaustive list of proposed copper-free formulations in market and industrial levels.

Source	Level of development	Disclosed information about its formulation
(Bosch, 2021)	Available in market	Ceramic brake pad with copper replaced by a special aerospace alloy with high aluminium content*
(Fras-le, 2021)	Available in market	Not disclosed*
(Hella-Pagid, 2021)	Available in market	Not disclosed*
(Bendix, 2021)	Available in market	Ceramic brake pad*
(Leonardi, 2020)	Research level	Combination of steel fibres and barite using a reference market Cu-full masterbatch
(Bhatt et al., 2021)	Research level	Copper replaced by iron-aluminum (FA25) alloy particles
(Kalel et al., 2021)	Research level	Copper replaced by stainless steel particles
(Tavangar et al., 2020)	Research level	Copper replaced by thermo-graphite and cellulose fibres
(Aranganathan, 2015)	Research level	Copper replaced by thermo-graphite
(Mahale, 2019)	Research level	Copper replaced by stainless steel swarf
(Hu, 2016)	Research level	Copper replaced by metal composites (Zn, Fe)

* Sources used: fabricants' websites and online selling platforms, such as Amazon.

Besides the technical advances in research, there is a need to progress in legislation. To date, the United States has pioneered the creation of a law limiting copper in automotive brake pads. Additional efforts from other countries must be made to spread this law elsewhere. To raise awareness of brake pads consumers, legislation must be drawn up by responsible environmental bodies to support this engagement.

5. CONCLUSIONS

Combining the CoF results with the characterisation results, and by analysing current trends for copper-free brake pads, the following conclusions are drawn:

- The copper tribotests presented a mean value of the coefficient of friction between 0.6 and 0.7, with a high standard deviation. On the other hand, the tests with brass and aluminium pins presented fewer oscillations of the coefficient of friction, with mean values rotating around 0.3 and 0.4 respectively, but with higher oscillations after a considerable test time.
- The EDS elemental mapping showed that the oxygen concentrations reached considerable values in regions coinciding with the material from each pin (less expressive for brass pins). This leads to the hypothesis of oxidation of the adhered material and the formation of a tribofilm that softened the coefficient of friction behaviour after the running-in phase, as other studies also suggested.
- Brass pins were the most worn for every normal load applied. In addition, debris formation for brass pins was visually much larger than for copper and aluminium pins. The brass pins showed a tribofilm more opaque and crisp than the other two types of pins.
- The tests for the three tribopairs followed the same trends: the increase in the normal load applied implied an increase in the loss of pin mass and a decrease in the mean coefficient of friction. However, the second trend is not statistically proven because of the high standard deviation.
- Laboratory experiments have their role in the development of copper-free formulations. However, it is remarkable that due to the many constituents in the brake friction materials, the complexity of the phenomena in friction is difficult to predict and interpret. The influence of other testing parameters must be evaluated, such as temperature, atmosphere composition and sliding speed.
- More and more, eco-friendly products are demanded by the market, and a critical selection of the constituents and the evaluation of emissions must be considered more carefully. The future of copper-free formulations for brake pads in Brazil remains uncertain.

6. REFERENCES

ABASSI, S. **A study of airborne wear particles generated from organic railway brake pads and brake discs**. Wear, 273 (2011) 93-99. Available at:

<https://doi.org/10.1016/j.wear.2011.04.013>

Aranganathan, N. **Special grade of graphite in NAO friction materials for possible replacement of copper**. Wear, 330 (2015). 515-523. Available at:

<https://doi.org/10.1016/j.wear.2014.12.037>

ARANGO, C.C.V. **Transição no regime de desgaste por deslizamento dos aços: uma abordagem termodinâmica.** Thesis (PhD in Mechanical Engineering) - Escola Politécnica da USP, p.250, 2010.

ASTM (2011). **Standard Test Method for Wear Testing with a Pin-on-Disk Apparatus**. ASTM International, (Reapproved 2010), 1–5. Available at:

<https://doi.org/10.1520/G0099-05R10.2>

BHATT, B. et al. **Fe–Al alloy for eco-friendly copper-free brake-pads**. Tribology International, 163 (2021) 107156. Available at:

<https://doi.org/10.1016/j.triboint.2021.107156>

BENDIX. **Bendix Premium, 2021**. Bendix Premium brake pad web page. Available at: http://www.bendix-brakes.com/bendix_premium.php. Access on: 30/10/2021.

BLAU, P.J. **Friction science and technology**. CRC Press. 1996

BOSCH. **Bosch Copper-Free, 2021**. QuietCast brake pad web page. Available at: <https://www.boschcopperfree.com/en/>. Access on: 30/10/2021.

BOUCHOUCHA, **A. Metals transfer and oxidation of copper—steel surfaces in electrical sliding contact.** Surface and Coatings Technology (1995), 76-77, 521–527. Avaialble at:

<https://doi.org/10.1016/0257-8972(95)02603-7>

BUSHAN, B. **Introduction to tribology,** John Wiley & Sons, Ltd. 2002

CALIFORNIA DEPARTMENT OF TOXIC SUBSTANCES CONTROL. **Limiting Copper in Brake Pads**. Available at: <https://dtsc.ca.gov/scp/limiting-copper-in-brake-pads/>. Access on: 30/10/2021.

CHOWDHURY, M. A., KHALIL, M. K., NURUZZAMAN, D.M. & RAHAMAN, M. L. **The effect of sliding speed and normal load on friction and wear property of aluminium.** (2011) International Journal of Mechanical and Mechanics Engineering, 11(1), 53–57

CZICHOS, H. **Systems approach to wear problems.** Wear control handbook (1980) 17-34.

CES EDUCPACK. Version 2015, 1.0. CES, 2015. Available at: <https://www.grantadesign.com/news_articles/ces-edupack-2015-materials-education-software-supports-teaching-for-real-world-engineering/>. Access on: 07/01/2021.

FERNANDES, G.P. **Aplicação da Tribologia na Pesquisa e Desenvolvimento de Materiais para Embreagens Automotivas: estudo do atrito e do desgaste com foco na origem do desenvolvimento, estabilidade e deterioração do tribofilme.** Thesis (PhD in Mechanical Engineering) - Escola Politécnica da USP, p.394, 2016.

FERREIRA, R.F (2017). **Caracterização microestrutural de pinos e discos metálicos após ensaio tribológico do tipo pino versus disco.** Master thesis, 160f. Universidade de São Paulo, 2017.

FRAS-LE. **Fras-le copper-free brake pad**, 2021. GRN Tech brake pad web page. Available at: < https://www.fras-le.com/us-ca/noticias/fras-le-copper-free-brake-pad/>. Access on: 30 de out. de 2021.

GALVANI, G.B. (2017). **Ensaios tribológicos do tipo pino versus dico para quarto pares metálicos: caracterização microestrutural dos tribofilmes e tribosuperfícies.** PIBIC scientific initiation report. Universidade de São Paulo, 2017.

HALLING, J. **Introduction to tribology.** Wykeham Publications. 1976.

HELLA-PAGID. **Hella Pagid copper-free brake pad**, 2021. Brake pad web page. Available at: <https://www.hella-pagid.com/hellapagid/en/Copper-free-brake-pads-613.html>. Access on: 30/10/2021.

HU, B. **Friction and Wear Responses with Metallic Composite Materials to Replace Copper and Copper Alloys in Brake Pad Formulations**, SAE Technical Paper, 2016. Available at:

<https://doi.org/10.4271/2016-01-1912>

ISO (2012). **Geometrical product specifications (GPS) — Surface texture: Areal — Part 2: Terms, definitions and surface texture parameters**. Available at:

<https://www.iso.org/standard/42785.html>

JACKO, M.G ; TSANG, P.H.S and RHEE, K. **Automotive friction materials evolution during the past decade.** Wear (1980), 100, 1984. 503-515.

KALEL, N. **Copper-free brake-pads: A break-through by selection of the right kind of stainless steel particles**. Wear (2021), 464-465, 203537. Available at:

<https://doi.org/10.1016/j.wear.2020.203537>

KATO, H; KOMAI;H. **Tribofilm formation and mild wear by tribo-sintering of nanometer-sized oxide particles on rubbing steel surfaces.** Wear 262 (2007) 36-41. Available at:

<https://doi.org/10.1016/j.wear.2006.03.046>

KATO, H. **Effects of supply of fine oxide particles onto rubbing steel surfaces on severe-mild wear transition and oxide film formation.** Tribology International 41 (2008) 735-742. Available at:

<https://doi.org/10.1016/j.triboint.2008.01.001>

KUKUTSCHOVA, J.; ROUBICEK, V.; MALACHOVVA, K.; PAVLICKOVA, Z.; HOLUSA, R.; KUBACKOVA, J.; MICKA, V.; MACCRIMMON, V.; FILIP, P. **Wear mechanism in automotive brake materials, wear debris and its potential environmental impact.** Wear, 267 (2009) 807-817. Available at:

<https://doi.org/10.1016/j.wear.2009.01.034>

LEONARDI, M. **Development of novel eco-friendly friction materials for disc brake systems.** Doctoral thesis. Università di Trento, 2020.

MALEQUE, M.A.; DYUTI, S.; RAHMAN, M.M. **Material selection method in design of automotive brake disc.** Proceedings of the World Congress on Engineering 2010 Vol. III. WCE 2010, June 30 - July 2, London, U.K., 2010.

MAHALE **A step towards replacing copper in brake-pads by using stainless steel swarf**. Wear (2019), 424-425, 133-142. Available at:

<https://doi.org/10.1016/j.wear.2019.02.019>

MUTALIB, M.A. **Scanning Electron Microscopy (SEM) and Energy-Dispersive X-ray (EDX) Spectroscopy.** Membrane Characterisation (2017), 161-179. Available at:

<https://doi.org/10.1016/B978-0-444-63776-5.00009-7>

PEREIRA, H. B. (2014). **Ensaio pino sobre disco do latão 270, 260 e do cobre sobre aço H13**. São Paulo: Escola Politécnica da Universidade de São Paulo, 2014.

OLOFSSON, U; GIALANELLA, S.; WAHLSTROM, J.; LEONARDI, M; LYU, Y. **Friction, wear and airborne particle emission from Cu-free brake materials.** Tribology International (2020), 141, 105959. Available at:

<https://doi.org/10.1016/j.triboint.2019.105959>

ÖSTERLE, W. **Chemical and microstructural changes induced by friction and wear of brakes**. Wear, 251 (2001) 1469-1476. Available at:

<https://doi.org/10.1016/S0043-1648(01)00785-2>

ÖSTERLE, W.; PRIETZEL, C.; KLOß, H., & DMITRIEV, A. I. **On the role of copper in brake friction materials.** Tribology International (2010), 43. Available at:

<https://doi.org/10.1016/j.triboint.2010.08.005>

RODRIGUES, A.C.P. **Effect of Cu particles as an interfacial media addition on the friction coefficient and interface microstructure during (steel/steel) pin on disc tribotest**. Wear (2015), 330-331, 70-78. Available at:

<https://doi.org/10.1016/j.wear.2015.02.006>

RODRIGUES, A.C.P. **Pin-on-Disc Tribotests With the Addition of Cu Particles As An Interfacial Media: Characterisation of Disc Tribosurfaces Using SEM-FIB Techniques.** Tribology International (2016), 100, 351-359. Available at:

<https://doi.org/10.1016/j.triboint.2016.03.034>

RODRIGUES, A.C.P. **Impact of copper nanoparticles on tribofilm formation determined by pin-on-disc tests with powder supply: Addition of artificial third body consisting of Fe3O4, Cu and graphite**. Tribology International (2017), 110, 103-112. Available at:

<https://doi.org/10.1016/j.triboint.2017.02.014>

SAMAD, M.A.; FELLAH, M.; SAYAH, T.; BENOUALI, C.; BEY, M.N.B.; BOUGOFFA, M.S.E. **Dry sliding friction and wear behaviour of CuZn39Pb2 and AA7075 under industrial and laboratory conditions.** Journal of Bio- and Tribo-Corrosion (2021). Available at:

<https://doi.org/10.1007/s40735-021-00475-x>

STACHOWIAK, G.W.; BATCHELOR, A.W. **Engineering tribology,** Butterworth Heinemann, 2001.

STRUERS. **Vickers hardness testing,** 2021. Struers web page. Available at: <https://www.struers.com/en/Knowledge/Hardness-testing/Vickers#introduction>. Access on: 07/11/2021.

TAYLOR ROBSON. **What is a Surface Profiler & Profilometer Working Principle**, 2018. Taylor Robson web page. Available at: <https://www.taylor-hobson.com/resource-center/blog/2018/july/what-is-a-surface-profiler>. Access on: 07/11/2021

TAVANGAR, R. **Comparison of dry sliding behavior and wear mechanism of low metallic and copper-free brake pads**. Tribology International (2020), 151, 106416. Available at:

<https://doi.org/10.1016/j.triboint.2020.106416>

ZUM GAHR, K. H. **Microstructure and Wear of Materials**. Elsevier, 1987.